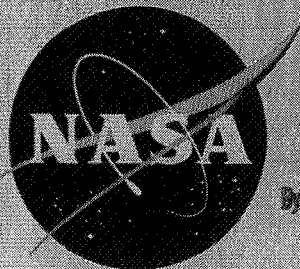


Copy 575

~~CONFIDENTIAL~~

NASA TM X-605

NASA TM X-605



CLASSIFICATION CHANGED
UNCLASSIFIED

TO _____
By Authority of TD 71-635 Date 18 OCT 1971

TECHNICAL MEMORANDUM

X-605 Declassified by authority of NASA
Classification Change Notices No. 215
Dated 21 DEC 1971

INVESTIGATION OF THE COMPRESSION FIELD AND THE
FLOW DISTRIBUTION IN THE THROAT OF A TWO-DIMENSIONAL,
INTERNAL-COMPRESSION, MACH NUMBER 6.9 INLET

By John R. Henry, Ernest A. Mackley,
and Marvin G. Torrence

Langley Research Center
Langley Air Force Base, Va.

[REDACTED]

[REDACTED]

NATIONAL AERONAUTICS AND SPACE ADMINISTRATION
WASHINGTON November 1961

~~CONFIDENTIAL~~

W

L
1
6
4
3

NATIONAL AERONAUTICS AND SPACE ADMINISTRATION

TECHNICAL MEMORANDUM X-605

INVESTIGATION OF THE COMPRESSION FIELD AND THE
FLOW DISTRIBUTION IN THE THROAT OF A TWO-DIMENSIONAL,
INTERNAL-COMPRESSION, MACH NUMBER 6.9 INLET*

By John R. Henry, Ernest A. Mackley,
and Marvin G. Torrence

SUMMARY

An investigation of a two-dimensional, internal-compression inlet designed to operate at a Mach number of 6.9 was conducted at a Mach number of 6.82 and a test-section Reynolds number per foot of 3.35×10^6 . The model had provisions for several configurations of boundary-layer bleed holes and slots and for variable geometry to change the contraction ratio. Pitot-stagnation-pressure and static-pressure surveys were made to determine the flow distributions in the throat. A maximum contraction ratio of 26.1, an average pitot-pressure recovery in the throat of 33.8 percent, and a total bleed flow of 6.1 percent of the capture mass flow were obtained with a boundary-layer bleed configuration consisting of holes and slots in the sidewalls and slots in the edges of the movable portions of the compression surfaces. Closing the slots in the compression surfaces resulted in a maximum contraction ratio of 20.2, an average pitot-pressure recovery in the throat of 29 percent, and a total bleed flow of 1.7 percent of the capture mass flow. In both cases the average corrected total-pressure recovery was approximately 50 percent and the maximum point value of Mach number at the throat was 2.5. With a fixed boundary-layer bleed configuration consisting of center-line slots and holes in the sidewalls, additional bleed through holes in the sidewalls substantially upstream from the throat produced a larger increase in recovery per unit increase in bleed flow than boundary-layer removal through the slots in the edges of the movable compression surfaces.

INTRODUCTION

Relative to flight at hypersonic speeds, many design studies have shown that the high values of the fuel-specific-impulse characteristic

*Title, Unclassified.

of air-breathing propulsion units would provide vehicle performance levels sufficient to accomplish many missions of both civilian and military value (for example, ref. 1). Research and development in many critical areas are required before such vehicles will become a reality (refs. 1, 2, and 3); one of these areas is hypersonic inlets. Some general considerations of hypersonic inlet performance are presented in references 4 and 5. Representative data for both fixed- and variable-geometry, axisymmetric, spike inlets in the Mach number range from 4 to 8 are presented in references 6 to 10. A discussion of high-temperature effects on inlet performance in the Mach number range from 8 to 15 is also presented in reference 10.

Most hypersonic inlet applications require variable-geometry capabilities for which two-dimensional inlets are well suited. The exploratory investigation reported herein consisted of the determination of the viscous effects on the hypersonic and supersonic compression field of a two-dimensional, internal-compression inlet at a nominal free-stream Mach number of 6.82. The complete inlet design includes a pitot-type center body with a boundary-layer bypass around the leading edge, which is to be located at the inlet throat. The present investigation included an experimental determination of the flow conditions at the throat location which was needed in order to design the center body.

The data presented represent results obtained from static-pressure measurements on the sidewalls and compression surfaces and from total- and static-pressure surveys at the throat station for a range of contraction ratios and for several configurations of boundary-layer bleed holes and slots on the sidewalls and compression surfaces. The investigation was conducted in the Langley 11-inch hypersonic tunnel at a Mach number of approximately 6.82, a stagnation pressure of 24.5 atmospheres absolute, and a stagnation temperature of 1,100° R. These conditions correspond to a Reynolds number per foot of 3.35×10^6 . The inlet capture area was a 2- by 4-inch rectangle, which corresponds to a model scale of approximately 1/15. Based on the inlet height, the test Reynolds number was about 25 percent of the full-scale Reynolds number. The tests were conducted at zero angles of attack and yaw.

SYMBOLS

A	cross-sectional area, sq ft
l	distance from wall, in.
M	Mach number

m	mass flow, slugs/sec
n	exponent in boundary-layer equation, $\frac{u}{U} = \left(\frac{y}{\delta}\right)^{1/n}$
p	static pressure, lb/sq ft
p_t	total pressure, lb/sq ft
$p_{t,1}$	corrected total pressure, calculated total pressure upstream of pitot-tube normal shock wave, lb/sq ft
$p_{t,2}$	pitot stagnation pressure, lb/sq ft
s	length of flap slot measured from flap trailing edge (fig. 2)
U	velocity at edge of boundary layer, ft/sec
u	local velocity in boundary layer, ft/sec
x	longitudinal distance from leading edge, in. (fig. 1)
y	vertical distance from horizontal center line, in. (fig. 1)
z	lateral distance from vertical center line, in. (fig. 1)
Δ	incremental change
Δ^*	mass-flow defect area, sq ft
δ	boundary-layer thickness, in.

Subscripts:

b	boundary-layer bleed flow
max	maximum
T	throat station
∞	free stream

A bar over a symbol indicates an area-weighted average value.

APPARATUS AND TESTS

Hypersonic Tunnel

The Langley 11-inch hypersonic tunnel is a blowdown facility with a maximum running time of about 1 minute. Flow characteristics of the nozzle and test section are presented in reference 11, which states that a region approximately 5 by 5 inches in the center of the test section has uniform parallel flow. The nominal Mach number of the flow was 6.82, the free-stream Reynolds number per foot was 3.35×10^6 , and the stagnation temperature was about $1,100^\circ \text{R}$.

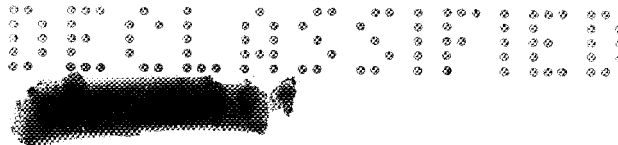
The assumptions that a full-scale inlet would have a capture height of 5 feet and that a flight Mach number of 6.82 would correspond to an altitude of 95,000 feet result in a full-scale Reynolds number of 4.45×10^6 . Thus, the 4-inch inlet height corresponds to a model scale of $1/15$ and the test Reynolds number of 1.12×10^6 is about $1/4$ of the full-scale value. Results given in reference 10 indicate that increasing the test Reynolds number beyond a value of 10^6 would not produce significant gains in performance.

For the test Reynolds number (3.35×10^6 per foot) and leading-edge bluntness (0.007-inch diameter) of the present model, the investigation of transition on the outside surface of a hollow cylinder made in the Langley 11-inch hypersonic tunnel (ref. 12) indicates that the length of laminar flow on a plate mounted in the test section would be about 11.8 inches and the transition Reynolds number would be 4×10^6 . The length of laminar flow on the inside surface of the inlet model should have been much shorter because of the higher Reynolds number level and the adverse pressure gradient; therefore, the boundary layer should have become turbulent well upstream of the inlet throat.

Model Description

The internal-compression inlet model used for the tests (figs. 1 to 3) was two dimensional with the internal width constant at 2 inches. The capture height was 4 inches and the design throat height was 0.170 inch. The overall model length was 37.7 inches; the design contraction ratio A_∞/A_T of 23.5 was accomplished in 13.269 inches. The model sidewalls were cut back at an angle of $120^\circ 36'$ with the free stream (fig. 1) to increase the ease of starting the inlet and decrease the amount of sidewall wetted area.

The variable geometry needed for starting and running contractions was provided by hinging the compression surfaces at $x = 7.824$ inches.



The movable portions downstream of this station are referred to as flaps (fig. 2). The model was designed for the addition of a pitot-type inlet center body to be located just downstream from the ends of the flaps, as shown by the dashed outline in figure 1. The frontal size of the center body or amount of boundary layer bypassed is to be determined from the present tests.

Sidewall boundary-layer bleed was provided by the use of 1/8- and 1/16-inch-diameter holes drilled at 15° to the inside surfaces in the area of $x = 7.824$ inches and $x = 11.52$ inches, respectively, and a slot in each sidewall located symmetrically along the horizontal midplane of the inlet, as shown in figure 1. The front sets of bleed holes were provided with removable external covers in order to obtain data with and without bleed in this area. The rear portion of each of the flaps had the edges relieved to form boundary-layer bleed slots between the flaps and sidewall, which could be closed by inserting filler pieces (fig. 2). In one set of tests, the slots were left approximately half open by cutting off the downstream portion (1.076 inches) of the filler pieces. A summary of the model configurations tested is presented in the following table:

Configuration	Boundary-layer bleed configuration			
	Sidewall			Flap slots
	Holes		Center-line slot	
	1/8-inch diam.	1/16-inch diam.		
I	Open	Open	Open	Closed
II	Closed	↓	↓	Open
III	Open			Open
IV	Closed			Closed
V	Open			Approx. half open

The 1/16-inch-diameter holes located at $x = 11.52$ and 11.77 inches and the center-line slots located between $x = 10.344$ and 12.944 inches (fig. 1) were open for all configurations. Changes from one configuration to another were made by opening or closing the 1/8-inch-diameter holes and the flap slots except for configuration V, which had open 1/8-inch-diameter holes and approximately half-open flap slots (fig. 2).

Model Aerodynamic Design

As previously noted, the sidewall was cut back to form an angle of $12^{\circ}36'$ with the free stream (design angle of first shock wave was $10^{\circ}22'$) giving a Mach number component normal to the leading edge of 1.49 for $M_{\infty} = 6.82$. The angle of the sidewall leading edge was set at a higher value than the first shock angle in order to be able to fix the sidewall wedge angle at 11° in a plane normal to the sidewall leading edge; 11° is low enough to have leading-edge shock-wave attachment (with zero leading-edge thickness) and high enough to present no difficulty in machining the surface. Since the leading edge was blunted to a 0.007-inch thickness, the leading-edge shock was detached slightly. For a model scale of 1/15 the corresponding full-scale leading-edge thickness would be only 0.10 inch; therefore, the model leading edge is considered to simulate a sharp leading edge.

Analyses of ramjet cycles and range-weight computations show that a total-pressure recovery of approximately 25 percent (kinetic-energy efficiency of 0.95) would be satisfactory at a Mach number of 6.9. In order to provide an allowance for boundary-layer bleed drag and viscous effects, the theoretical overall total-pressure recovery of the complete inlet was fixed arbitrarily at 42 percent. For a free-stream Mach number of 6.9, a series of 16 two-dimensional shocks of 3° turning angle followed by a terminal normal shock at a Mach number of 2.62 produces a theoretical total-pressure recovery of 42 percent. The compression field up to the inlet throat was to contain 14 of the 3° shocks, and the pitot-type center body was to contain the remaining two 3° shocks and the normal shock. The present investigation is concerned with the flow field up to the inlet throat with no center body in place; the theoretical total-pressure recovery up to the throat station with a normal shock at a Mach number of 2.91 included is 33 percent.

The initial design consisted of an arrangement of 14 shocks, each turning the flow 3° , in the forward part of the inlet as indicated in figure 4(a). The aerodynamic compression was symmetrical about the horizontal midplane of the inlet with a series of seven shocks originating on each compression surface and coalescing on the trailing edge of the opposite compression surface (flap) at $x = 13.269$ inches where the shocks were canceled on a sharp corner, theoretically giving uniform flow in the throat parallel to the center line. Because of anticipated boundary-layer effects, the corner was rounded (0.060-inch radius). Focusing the compression on a corner produces a relatively short inlet at the cost of a high adverse pressure gradient in the boundary layer near the corner. Since a boundary-layer bypass around the periphery of the leading edge of the center body was included in the design and since the canceling corner was rounded, this pressure gradient was not considered to be a serious disadvantage.



L
1
6
4
3


In the final design, the compression surface upstream of the flaps was not changed from the two discrete flat surfaces but the contour of the flap surfaces was faired to a smooth curve for ease in machining. Figure 4(b) shows the compression field (nonviscous) recomputed for $M_\infty = 6.85$ with the curved flap surfaces at a contraction ratio of 26.1 (sharp canceling corner), the highest obtained in the present tests. The isentropic compression waves originating on the curved flap surfaces were computed by the two-dimensional characteristics method with the waves being taken at 2° intervals of turning. The shock waves and the coalescing 2° isentropic compression waves meet the flap surface ahead of the canceling corner. Similar analyses of the flow at a Mach number of 6.85 and for lower contraction ratios showed that the majority of the shock and isentropic waves would hit the corner at a contraction ratio of about 22.9; this contraction ratio produces a uniform Mach number of 2.86 over most of the throat height.

Instrumentation

The model pressure instrumentation consisted of eight static-pressure orifices in the sidewall, located as shown in figure 4(b). The first seven were installed to measure the pressure rise through the first seven compression waves in the original design and the eighth was to measure the throat static pressure on the sidewall. Four static-pressure orifices were staggered down the center line of the inside surface of the top flap and three static-pressure orifices were located across the downstream end of the flap (fig. 2).

Figure 5 shows the three-tube pitot-pressure rake and the two-tube static-pressure rake used to make total- and static-pressure surveys at $x = 13.238$ inches by rotating the rake support. The rake tubes moved through a maximum arc of about $\pm 10^\circ$ in the Y-plane with the axis of rotation located in the horizontal midplane of the inlet. The transverse position z of the pitot rake was changed between tests by repositioning clamps on the rake shaft outside the model sidewall (fig. 5). The static-pressure surveys were made only at one transverse position which gave surveys in the Y-plane for values of z of ± 0.485 .

The pitot- and static-pressure surveys at the throat were recorded by pressure transducers and electronic-data plotters with the rake movement on one axis. All other pressures were recorded on six-cell flight-type pressure recorders (ref. 13) or pressure transducers in conjunction with electronic strip chart recorders. The pressure transducers and associated recorders used were limited to a maximum frequency response of about 10 cycles per second. The tunnel stagnation pressure remained nearly constant during the runs but was recorded every 10 seconds from a precision Bourdon gage. Schlieren pictures were taken of the inlet model with the tunnel flow established.



Tests

The model was cooled to near room temperature before each test because the running inlet contraction ratio A_{∞}/A_T was found to be not as high for an initially hot (200° F to 300° F) model as for a cooled (90° F to 110° F) model. This effect was considered to be a boundary-layer growth effect but was not investigated further. The same phenomena were observed in the investigation described in reference 10, which presents data on the maximum contraction ratios obtainable for cooled and uncooled model walls.

With regard to boundary-layer development in the inlet, it is desirable to conduct model tests at the same ratio of actual wall temperature to adiabatic wall temperature that would be encountered in flight. For several tests in the subject investigation, the inner wall surface temperature was measured at a point three-eighths of an inch downstream from the pivot point on the lower flap. The measured temperature reached a value of approximately 600° R at the end of the tests. For the Mach number of 5.49 in this region, the tunnel stagnation temperature of 1,114° R, and turbulent flow, the measured wall temperature corresponds to a ratio of actual wall temperature to adiabatic wall temperature of 0.59. If flight is assumed to be at a Mach number of 6.82, at an altitude of 95,000 feet and in a perfect gas, the same ratio of actual wall temperature to adiabatic wall temperature would correspond to a wall temperature of 1,810° F, which appears to be a reasonable operating temperature. Therefore, the ratio of model wall temperature to adiabatic wall temperature was of the same order as that to be expected in flight.

In a typical test, the data recorders were turned on, the tunnel flow was established, and the flaps were closed to a predetermined contraction ratio. If the inlet remained started as shown by visual observation of continuous schlieren images, the pitot- or static-pressure survey at the throat was made. For some tests complete surveys were made in both +y and -y directions to check the response of the instrumentation. For some of the boundary-layer bleed configurations, static-pressure surveys were omitted for some of the contraction ratios for which pitot-pressure surveys were made. In these cases the static-pressure data were obtained by interpolation between the data for other contraction ratios. The contraction ratios tested for each boundary-layer bleed configuration are summarized in the following table:

L
1
6
4
3

Configuration	Contraction ratio, A_{∞}/A_T											
	29.8	26.1	23.5	22.5	20.2	19.0	15.8	13.5	12.1	11.0	9.7	9.0
I				U	T, S	T		T	T, S	T	T, S	T
II					T, S		T, S		T, S			
III	U	T, S	T, S		T, S							
IV						U	T, S				T, S	
V					T							

The letter U indicates that the flow was unstable and the inlet would not remain started for the particular configuration and contraction ratio. This condition was definitely established for configurations I, III, and IV only. The letters T and S indicate that total- and static-pressure surveys, respectively, were made for the particular contraction ratio and configuration. The z-locations of the survey tubes are given in figure 5.

DATA PROCESSING

Survey Data

The data from the static- and pitot-stagnation-pressure surveys at the throat station were processed to determine pitot pressure, corrected total pressure, mass flow per unit area, and Mach number distributions. Corrected total pressure is defined as the calculated total pressure upstream of the pitot-tube normal shock wave. The data obtained with the two static-pressure survey tubes (figs. 3(a) and 5), which were located symmetrically in the throat at values of z of ± 0.485 inch, agreed at all values of y and were averaged arithmetically. The assumption was made initially that the measured static-pressure distributions applied to all the z -locations of the pitot-pressure surveys. Processing representative samples of the data on this basis resulted in corrected total-pressure recoveries which exceeded 100 percent at many locations. The overall conclusion derived from the pitot- and static-pressure surveys is that the static-pressure surveys were made at z -locations corresponding to minimum static-pressure regions. Subsequently, it has been determined that this result may have been due to disturbances originating at the sidewall boundary-layer bleed slots at points where shocks from the compression surfaces cross the horizontal center line. The flow would be expected to turn into the slot at a steeper angle at such locations and, as a result, a fan of expansion waves extending into the inlet flow towards the throat station would be produced. A fan of expansion waves originating at the slot at

$x = 10.79$ inches (intersection of leading-edge shocks with horizontal center line, fig. 4(b)) would cross the throat station at the static-pressure-survey tube location z of ± 0.485 inch.

In order to process the data, a systematic procedure for estimating the static pressures at the z -locations of the pitot-pressure surveys was developed. For each z -location of the pitot-pressure surveys, a static-pressure correction factor was determined which, when applied to the static-pressure survey data at all y -locations and combined with the particular pitot survey data to determine the corrected total pressures, would result in a corrected total-pressure recovery which did not exceed 95 percent at any y -location in the pitot survey. The 95 percent value of corrected total-pressure recovery was determined to be a reasonable maximum value from a study of shock diagrams. For each boundary-layer bleed configuration, the static-pressure correction factors were plotted as a function of z for constant values of contraction ratio with symmetry assumed about the vertical center line of the throat, and families of curves were faired through the higher values of correction factor so that a conservative result relative to corrected total pressure was produced. Examples of the faired curves are presented in figure 6 for configurations I and III. Data derived from the flap static-pressure orifices were also utilized in fairing the curves as indicated in the figure. The value of the correction factor is not necessarily 1.0 at the static-pressure survey station ($z = 0.485$ inch) because the curve fairings were determined primarily by the trend of the correction-factor point values.

L
1
6
4
3

The maximum static-pressure error obtained by this procedure is estimated to be about 30 percent of the difference between the corrected and measured static pressures, which error figure 6 indicates to be a maximum of approximately ± 15 percent. Figure 7 presents calculated errors for point values of mass flow per unit area, Mach number, and corrected total pressure corresponding to a static-pressure error of ± 15 percent. The curves indicate that mass flow is not sensitive to the high static-pressure error, whereas corrected total pressure may have large errors at the higher Mach numbers.

Bleed-Flow Computations

Bleed-flow quantities through the bleed holes and slots shown in figure 1 were computed for all tests with the assumption that the total pressure of the bleed flow was equal to the static pressure of the inlet internal flow at the location of the particular hole or slots. When it was assumed that the external ambient pressure corresponded to that downstream of the external shock on the sidewall leading edge, the total pressure of the bleed flow in every case was considerably in excess of that required to choke the bleed passage (Mach number of 1.0 in the passage). Orifice coefficients of 0.65 for the bleed holes and 1.00 for

the bleed slots were assumed. At the bleed-hole and flap-slot locations, the static pressures of the inlet internal flow were determined from the wall static-pressure measurements. In the case of the center-line bleed slots, the static pressures were computed from flow diagrams similar to figure 4(b).

RESULTS AND DISCUSSION

Flow Observations

L
1
5
4
3
Schlieren pictures of the shock pattern and boundary-layer development in the inlet are presented in figures 8(a) and 8(b) for configuration I and a contraction ratio of 20.2. The observation of the shock formation in the internal flow of the inlet was possible due to the unobstructed views through the center-line bleed slots and the 1/8-inch bleed holes. Near the leading edge of the center-line slot the schlieren picture shows a single shock which was produced by one of the static-pressure orifice lines mounted on the outer surface of the model. Downstream from the single shock three X-shocks are visible which originated at the compression surfaces. The upstream legs of the first X-shock are visible at the outer edge of the second bleed hole from the center line in the upstream row of bleed holes on both the top and bottom halves of the model. Also, in the upstream row of bleed holes the views of the top and bottom holes show that the flow is all boundary layer at these locations. Some of the pictures taken during the test show the edge of the boundary layer to be located at the outer edges of the top and bottom holes of the downstream row, which fixes the apparent thickness of the boundary layer in this area. Those several observations are indicated by the dashed lines in the diagram of figure 9.

A comparison of the theoretical shock pattern with the observed one indicates that the first X-shock in the center-line slots corresponds to the second shock originating on the compression surfaces (fig. 9). The actual shock, however, was displaced upstream from the theoretical location by approximately 0.35 inch because of the growth of the boundary layer on the compression surfaces. The second X-shock corresponds to the third shock originating on the compression surfaces, and the upstream displacement is approximately 0.24 inch. The third X-shock visible in the center-line slot apparently represents a focusing of Mach waves similar to those shown on figure 4(b). The apparent boundary-layer thickness at the bleed-hole location is approximately 0.12 inch, and from the diagram this thickness appears to be sufficient to displace the shock the indicated distances. Furthermore, the displacement distances are of the same order as the throat height, and thus the actual flow field in the vicinity of the throat would be expected to be substantially different from the theoretical one.

The growth of boundary layer along the inlet walls due only to flat-plate friction was computed in order to estimate the approximate location of transition from laminar to turbulent flow and in order to determine whether the flow at the throat station was entirely boundary layer. The effects on the boundary layer due to the adverse pressure gradient were ignored and no correction was made for boundary-layer bleed flow. The flow conditions at the edge of the boundary layer were assumed to be those indicated by the diagram of figure 4(b) for a contraction ratio of 26.1. Computations were made of the boundary-layer growth along the compression surface and along the horizontal center line of the sidewall for a constant wall temperature of 140°F and for adiabatic wall temperatures. In the actual tests, the wall temperatures probably were between these two temperatures since the walls in the vicinity of the throat would become hotter than 140°F because the throat region was subjected to lower Mach numbers and higher pressures than the region near the upstream end of the flap where the wall temperature of 140°F was measured. The methods outlined in reference 14 for laminar flow and in reference 15 (Eckert's) for turbulent flow and the tables of boundary-layer parameters given in reference 16 were utilized.

When the transition Reynolds number of approximately 4×10^6 previously discussed was used, the computations indicated that the transition would occur at the third shock on both the compression surface ($x = 7.93$ inches, fig. 4(b)) and on the sidewall at the horizontal center line ($x = 12.44$ inches). Boundary-layer thicknesses on the compression surfaces at the third shock location of 0.07 and 0.09 inch were computed for the wall temperature of 140°F and the adiabatic wall, respectively. Since the computations did not account for adverse pressure gradient, the computed thicknesses would be expected to be low. As previously discussed, figure 9 shows that the boundary-layer thickness was approximately 0.12 inch. The computations indicated that the boundary layers on the compression surfaces grew to the point where they extended across the entire flow at a station slightly upstream from the throat station. In the actual flow the boundary layer probably filled the duct at a station farther upstream than the computed one because of the effect of the adverse pressure gradient, which was not accounted for in the computations.

Longitudinal Static-Pressure Distributions

Typical wall static-pressure distributions obtained from the data for the sidewall and flap static-pressure orifices are presented in figures 10(a) to 10(c) together with theoretical curves for contraction ratios of 26.14 and 9.03, which were determined from shock diagrams similar to that in figure 4(b). All experimental and theoretical data are plotted as a function of a nominal turning angle in the compression

field, which corresponds to the location of the static-pressure orifices in figure 4(b) for a contraction ratio of 26.1. Therefore, as the contraction ratio is reduced below 26.1, the static pressure should also become lower because the turning angles are less than those indicated by the abscissa. The magnitude of this effect is shown by the difference between the theoretical curves, which correspond to the highest and lowest contraction ratios tested.

L
1
6
4
3

Up to a turning angle of about 8° , the data correspond to pressures which are appreciably above the theoretical values. This result may be due to the slight rounding of the leading edge on the sidewall and pressure transmission through the laminar boundary layer. Between turning angles of 9° and 20° the data from the flap static-pressure orifices are in good agreement with the theoretical data when allowances are made for the effects of boundary-layer bleed and reductions in contraction ratio; however, the sidewall static pressures did not decrease as much as is predicted by the theoretical curves for the sidewall because of boundary-layer effects. The data for the flap static pressures at a turning angle of 21° are considerably above the theoretical curve. This result is probably due to the shift of the flow pattern upstream due to boundary-layer growth; figure 4(b) shows that near the trailing edge of the flap, a shift in the compression field of 0.096 inch (from $x = 13.213$ to $x = 13.117$ inches) would change the angle of turning at the location of these orifices from 21.1° to 59.3° . Figure 9 shows that shifts in the compression field of two to three times this amount occurred in some areas. The sidewall static pressure in the vicinity of the throat at a turning angle of about 42° was affected significantly by the contraction ratio and the boundary-layer bleed configuration; however, the interpretation of these data is subject to question since the static-pressure orifice was located just downstream from the center-line bleed slot and just upstream from the large opening in the sidewall (fig. 1).

Boundary-Layer Bleed Flows

The ratio of boundary-layer bleed flow to the capture mass flow is presented as a function of contraction ratio and boundary-layer bleed configuration in figure 11. The total bleed flow ranged from about 1.0 percent of the capture mass flow for configuration IV (1/8-inch-diameter holes and flap slots closed, 1/16-inch-diameter holes and center-line slots in sidewall open) to about 6.1 percent of the capture mass flow for configuration III (all holes and slots open). As the contraction ratio was increased, the local static pressure at the bleed holes and slots increased which resulted in some increase in the amount of bleed flow. The range in the amount of bleed flow through the various holes and slots is approximately as follows:

Bleed passage	Bleed flow, percent	A_{∞}/A_T
1/16-inch-diameter holes	0.07 to 0.08	9.03 to 26.14
1/8-inch-diameter holes	0.25 to 0.27	9.03 to 26.14
Center-line slots	0.82 to 1.66	9.03 to 26.14
Flap slots	3.30 to 4.12	12.12 to 26.14

Relatively little flow passed through the bleed holes as compared with that through the slots because the bleed holes were located in lower pressure regions and had less cross-sectional area. The cross-sectional area of the flap slots was 80 percent of that of the center-line slots; however, approximately three times as much flow passed through the flap slots because they were located in higher pressure regions.

L
1
6
4
3

Contour Maps of Parameters at Throat Station

Effect of contraction ratio.— Data from the total- and static-pressure surveys were processed and converted to contour maps of various parameters for the throat station. The effect of contraction ratio on pitot-stagnation-pressure contours and mass-flow-per-unit-area contours for configuration I is presented in figures 12(a) and 12(b), respectively. Comparisons of the pitot-pressure contours show that, as the contraction ratio is increased, the pitot-pressure recovery increases in all areas. The pitot-pressure contours for the highest contraction ratio ($A_{\infty}/A_T = 20.2$) exhibit a substantial central region in which the recovery is nearly constant. Similarly, the mass-flow-per-unit-area contours for a contraction ratio of 20.2 contain a substantial region of nearly uniform flow distribution. The pitot-pressure recoveries increase with increasing contraction ratio because the Mach number decreases and thus the total-pressure loss through the bow wave in front of the survey tube decreases. The more uniform distributions for a contraction ratio of 20.2 are believed to be a result of the flow field approaching the condition represented by figure 4(a), where the compression waves from the opposite surface focus on the flap trailing edges. For such an ideal condition the flow would be uniform and axial in the throat. For smaller contraction ratios or larger throat heights, the reflected waves would enter the throat at various distances from the flap trailing edge, and gradients in the flow parameters at the throat would be established. In all the plots of figures 12(a) and 12(b), bulges in the contours near the center of the sidewall indicate that a quantity of low-energy boundary layer has collected in this region. These phenomena are a result of the transverse pressure gradients upstream in the inlet compression field and have been observed by other investigators. The boundary-layer bleed configurations were not sufficient to eliminate these low-energy regions.

Contour plots, which are not presented herein, for the several boundary-layer bleed configurations and for a given contraction ratio exhibit no significant differences due to changing the bleed configuration. Opening bleed holes and/or slots, however, permitted operation at higher maximum contraction ratios. Figures 12(c) and 12(d) contain contour maps of pitot-stagnation-pressure recovery and mass flow per unit area for the highest contraction ratios tested for configurations I to IV. The plots show principally the same effects due to increasing contraction ratio as noted in figures 12(a) and 12(b). For contraction ratios of 23.5 and 26.1 the accumulation of low-energy boundary layer on the sidewall apparently resulted in a separated-flow region. However, these two contraction ratios have lower peak values of mass flow per unit area than those for contraction ratios of 15.8 and 20.2 which had no separated flow.

Corrected total pressure and Mach number.—Contours of corrected total pressure and Mach number for the maximum contraction ratios for configurations I and III are given in figure 12(e). Although point values of the corrected total pressure may be in error as much as 20 percent at a Mach number of 2.5 (fig. 7) and the Mach number may be in error as much as 13 percent, contour plots such as those of figure 12(e) are believed to be of considerable interest. The corrected total-pressure recovery varies from 60 percent to 90 percent for roughly half of the cross-sectional area, and large areas of low recovery were present near the sidewall. As the flow proceeded from the leading edges to the throat station, figure 12(e) shows clearly that substantial total-pressure losses occurred because of boundary-layer phenomena associated with the large amount of wetted area and the adverse pressure gradients. The Mach number range was from 2.0 to 2.5 over the major portion of the cross sections in both tests. However, the Mach 2.5 regions for the contraction ratio of 26.1 were less in extent than those for the contraction ratio of 20.2.

Integrated Values of Parameters at Throat Station

Mass flow.—The results of integrating the contour maps of mass flow per unit area are presented in figure 13 in terms of the mass flow ratios m_T/m_o and $(m_T + m_b)/m_o$ as a function of contraction ratio for all the boundary-layer bleed configurations. The data are presented as an indication of the accuracy of the static-pressure correction factor and its effect on the mass flow at the throat. The open symbols represent the integrated values, and the filled symbols represent the sum of the integrated throat mass flow and the computed bleed flows from figure 11. The maximum inaccuracies indicated are ± 4 percent of the capture mass flow. These results tend to justify the method adopted for estimating static-pressure variation with z at the throat and appear to agree with the estimates of errors given in figure 7.

Pitot-stagnation-pressure recovery.— The results of integrating the contour maps of pitot-stagnation-pressure recovery are given in figure 14 in terms of $P_{t,2}/P_{t,\infty}$ as a function of contraction ratio. The pitot-pressure recovery includes the total-pressure loss through the normal shock bow wave in front of the survey tube and can be measured accurately. The integrated value is considered significant because it furnishes a theoretical value for overall recovery corresponding to the condition in which a terminal normal shock would be located at the throat station and for which there would be no subsonic diffusion losses. A high value of pitot-pressure recovery indicates not only that the total-pressure losses through the supersonic compression are low but also that the supersonic compression has reduced the flow to a low supersonic Mach number.

A theoretical curve has been included in figure 14 which represents the theoretical recovery through a normal shock at the throat after the flow has been compressed isentropically through the contraction ratio indicated by the abscissa. Theoretical point values are plotted in figure 14 for the original design corresponding to the shock diagram of figure 4(a) and for a contraction ratio of 26.1 corresponding to the diagram of figure 4(b). The pitot recoveries of the theoretical points are somewhat less than the isentropic compression curve due to oblique-shock total-pressure losses. The test data correspond to recoveries which are lower than the theoretical values because of the boundary layer and oblique-shock total-pressure losses and because there were effects due to the boundary-layer bleeds. The data show clearly that at a given contraction ratio the boundary-layer bleed configuration had little effect on the recovery; the faired data are about 90 percent of the recovery shown by the theoretical curve. Configuration III, which had the highest maximum contraction ratio and a bleed flow of 6.1 percent of the capture mass flow, attained a pitot recovery of 33.8 percent at a contraction ratio of 26.1. Configuration I, which had a maximum contraction ratio of 20.2 and a bleed flow of 1.7 percent, attained a pitot recovery of 29 percent.

Corrected total-pressure recovery.— Average values of corrected total-pressure recovery derived from integrations of the contour maps are presented in the bottom half of figure 15 as a function of contraction ratio for the five boundary-layer bleed configurations. All the solid curves, which have been faired through the data points, exhibit the same trend; the corrected recovery decreases as the contraction ratio increases up to a value of between 12 and 15, and further increases in contraction ratio result in increases in the recovery. Normally, the recovery would be expected to decrease progressively as the contraction ratio is increased since the losses in recovery are due to boundary-layer growth in an adverse pressure gradient and to the shock waves.

Computations were made to determine whether the trend exhibited by the data was associated with the method adopted for processing the

L
1
6
4
3

static-pressure survey data. A one-dimensional analysis was made in which the average corrected total-pressure values were determined by using the integrated values of pitot stagnation pressure of figure 14, the area contraction ratio, and the ratio of the throat mass flow to the capture mass flow. The results of these computations are presented as the dashed curves in the bottom half of figure 15. The computed corrected total-pressure curves, which are independent of the static-pressure survey data, exhibit the same trend as the integrated values of total pressure. This result indicates that the shape of the data curves in figure 15 is not associated with errors in the determination of static-pressure distributions at the throat. Although a reasonable assessment is not possible because of insufficient data, there are several factors which could influence the trend of the curves - for example, the trend of improving recovery with increasing contraction may have been due to an increase in boundary-layer bleed flow combined with a redistribution of the bleed flow. The data curves for total-pressure recovery show that at the highest contraction ratios (configurations I, II, and III) the total-pressure recovery was of the order of 50 percent.

The average throat Mach numbers determined from the one-dimensional analysis are presented in the top half of figure 15. At the highest contraction ratios the average Mach number varied from 2.2 to 2.5, depending upon the boundary-layer bleed configurations.

Effect of boundary-layer bleed on total-pressure recovery.- Pitot-stagnation-pressure recovery and corrected total-pressure recovery for the maximum contraction ratios tested for each configuration are presented in figure 16 as a function of bleed mass flow. The upper plot is corrected total-pressure recovery and the lower plot is pitot-stagnation-pressure recovery. The configuration number is noted adjacent to each data point. For configuration changes from IV to II or from I to III the physical change in the model consisted of opening the flap slots; for changes from IV to I or II to III the 1/8-inch-diameter bleed holes were opened. As discussed previously, the principal effect of opening bleed holes or slots was to increase the maximum allowable contraction ratio. Therefore, the changes in recovery indicated by the data points, which occurred when a configuration change was made, involve the effects of two variables, bleed mass flow and contraction ratio.

The primary point of interest to be noted in figure 16 is the slopes of the lines joining the data points, which are given in the table for both the pitot-stagnation-pressure and corrected total-pressure recoveries. Opening the 1/8-inch-diameter bleed holes produced a much larger increase in recovery per unit of bleed-flow increase than opening the flap slots. For instance, for the corrected total-pressure recovery a curve of 2.2 resulted from changing from

configuration IV to II (opening flap slots) as compared with a curve slope of 21.2 from changing from configuration IV to I (opening 1/8-inch-diameter bleed holes).

Mass-Flow Defect Area At Throat Station

The ratio of mass-flow defect area to throat area which is defined as

$$\frac{\Delta^*}{A_T} = \int_0^{A_T} \left[1 - \frac{m/A}{(m/A)_{\max}} \right] \frac{dA}{A_T}$$

or

$$\frac{\Delta^*}{A_T} = 1 - \frac{m_T/A_T}{[(m/A)_{\max}]_T}$$

was determined for the conditions given in the section entitled "Tests" and is presented as a function of the contraction ratio in figure 17. All the curves for the several boundary-layer bleed configurations exhibit the same trend: an initial increase in Δ^*/A_T as the contraction ratio is increased, a peak value of Δ^*/A_T , and a region of decreasing Δ^*/A_T with increasing contraction ratio. If the defect area were due only to the boundary layer, the curves would be expected to rise continuously with increasing A_∞/A_T due to consequent increasing adverse pressure gradient. However, the definition of the defect area is such that nonuniformities in the distribution of mass flow per unit area arising from shock and compression-field patterns are included in Δ^*/A_T . A qualitative indication of the contribution to Δ^*/A_T due to the nonuniform compression field at the throat is given by the theoretical curve in figure 17, which is based on values obtained from diagrams similar to that of figure 4(b). The theoretical curve cannot be considered quantitative because the actual shock patterns would be expected to differ from the theoretical ones due to boundary-layer effects. The difference between the measured data values and the contribution due to the flow field would provide an indication of the part of Δ^*/A_T due to the boundary layer. The boundary-layer contribution is indicated qualitatively by the hatched region in the bottom part of figure 17, which shows that the mass-flow defect due to the boundary layer does increase with increasing contraction ratio or adverse pressure gradient. For the region of contraction ratio values near the design value of 23.53 of figure 4(a), the flow in the throat would be expected to be nearly all axial and the mass-flow defect to be mostly due to the



boundary layer. For this region, the lowest values of mass-flow defect area for the data of figure 17 are approximately 40 percent of the throat area.

Each data point given in figure 17 may be identified with a location in the throat corresponding to the point of maximum mass flow per unit area, which always occurred near the center of the throat. The Mach number, pitot-stagnation-pressure recovery, and corrected total-pressure recovery at the points at which maximum mass flow per unit area occurs are given in figure 18 as a function of contraction ratio. As the contraction ratio was increased from 9 to 26, the Mach number was reduced from a value of about 3.0 to a little above 2.0 and the pitot-stagnation-pressure recovery increased correspondingly from 23 percent to 54 percent. The variation of corrected total-pressure recovery was somewhat random.

For the maximum contraction ratios for configurations I, II, and III, it is reasonable to assume that the mass-flow defect area is equivalent to the compressible displacement area. This assumption permits the determination of the average boundary-layer-equation exponents n and the incompressible form factors $(n + 2)/n$ as follows:

Configuration	A_{∞}/A_T	n	$(n + 2)/n$
I	20.2	3.43	1.58
II	23.5	2.99	1.67
III	26.1	3.52	1.57

The values of form factor given show that the boundary layer on the average was distorted appreciably by the adverse pressure gradient since a value of 1.29 corresponds to a normal undisturbed turbulent boundary layer with an n value of 7 and since a value of 1.80 may correspond to a separated boundary layer. The mass-flow distributions given in figures 12(c) and 12(d) show further that there was considerable variation in the distributions around the periphery of the throat, indicating that the maximum local value of form factor was considerably higher than the average value; in fact, separated flow regions are located on the sidewall in figure 12(c). The purpose of the boundary-layer bypass to be located around the periphery of the leading edge of the pitot-type center body indicated in figure 1 is to remove the lowest energy portions of the boundary layer in order to avoid excessive total-pressure losses in the vicinity of the terminal normal shock.

SUMMARY OF RESULTS

An investigation of a two-dimensional, internal-compression inlet was conducted at a Mach number of 6.82 in the Langley 11-inch hypersonic tunnel at a test-section Reynolds number per foot of 3.35×10^6 . The capture area of the inlet was a 2-inch by 4-inch rectangle, and the model incorporated provisions for several configurations of holes and slots for boundary-layer removal and variable geometry for starting and for varying the contraction ratio. Total- and static-pressure surveys of the flow at the throat station were made to determine pressure and flow distributions. The principal results of this investigation are summarized as follows:

1. The growth of boundary layer along the inlet walls shifted the shock pattern upstream by distances comparable in magnitude to the throat height as determined from comparisons of the theoretical shock pattern with schlieren observations.
2. A maximum contraction ratio of 26.1 and a bleed flow of 6.1 percent of the capture flow were obtained with a boundary-layer bleed configuration consisting of two sets of holes and a center-line slot on each sidewall and slots along the edges of the movable compression surfaces; the corresponding average pitot-stagnation-pressure recovery at the throat was 33.8 percent. Closing the slots in the movable compression surfaces resulted in a bleed flow of 1.7 percent of the capture mass flow, a maximum contraction ratio of 20.2, and an average pitot-pressure recovery of 29 percent. In both cases the average corrected total-pressure recovery at the throat was approximately 50 percent and the maximum point value of Mach number was 2.5.
3. With a fixed boundary-layer bleed configuration consisting of center-line slots and holes in the sidewalls, additional bleed through holes in the sidewalls substantially upstream from the throat produced a larger increase in recovery per unit increase in bleed flow than boundary-layer removal through the slots in the edges of the movable compression surfaces.
4. Boundary layer filled the entire cross section of the throat, and low-energy boundary layer accumulated at the center of the throat sidewalls resulting in separated-flow regions in some cases. For the highest contraction ratios tested, the throat boundary-layer displacement area was approximately 40 percent of the throat area.

Langley Research Center,
National Aeronautics and Space Administration,
Langley Air Force Base, Va., August 21, 1961.

[REDACTED]

21

REFERENCES

1. Swihart, John M., and Henry, John R.: Hypersonic Cruise Vehicles. Ch. VI of Compilation of Papers Summarizing Some Recent NASA Research on Manned Military Aircraft. NASA TM X-420, 1960, pp. 87-105.
 2. Drake, John A.: Hypersonic Ramjet Development. Combustion and Propulsion Fourth AGARD Colloquium on High Mach Number Air-Breathing Engines, A. L. Jaumotte, A. H. Lefebvre, and A. M. Rothrock, eds., Pergamon Press (New York), 1961, pp. 71-83.
 3. Dugger, Gordon L.: Comparison of Hypersonic Ramjet Engines With Subsonic and Supersonic Combustion. Combustion and Propulsion Fourth AGARD Colloquium on High Mach Number Air-Breathing Engines, A. L. Jaumotte, A. H. Lefebvre, and A. M. Rothrock, eds., Pergamon Press (New York), 1961, pp. 84-119.
 4. Connors, James F., and Allen, John L.: Survey of Supersonic Inlets for High Mach Number Applications. NACA RM E58A20, 1958.
 5. Connors, James F., and Obery, Leonard J.: Some Considerations of Hypersonic Inlets. Combustion and Propulsion Fourth AGARD Colloquium on High Mach Number Air-Breathing Engines, A. L. Jaumotte, A. H. Lefebvre, and A. M. Rothrock, eds., Pergamon Press (New York), 1961, pp. 123-137.
 6. Stitt, Leonard E., and Flaherty, Richard J.: Experimental Investigation of a Mach 5 Isentropic Spike Inlet at and Below Design Speed. NASA TM X-4, 1959.
 7. Stitt, Leonard E., and Chubb, Donald L.: Investigation of Three Mach 7 External-Compression Axisymmetric Inlets From Mach 1.9 to 6.8. NASA TM X-413, 1960.
 8. Kepler, C. Edward: Performance of a Mach 4.0 Variable-Geometry Axisymmetric Inlet Having External-Plus-Internal Compression. R-1285-12 (Contract NOa(s) 55-133-c), Res. Dept., United Aircraft Corp., Sept. 1959.
 9. McLafferty, George H.: Hypersonic Inlet Studies at UAC Research Laboratories. Rep M-2000-113, United Aircraft Corp., Dec. 1959.
 10. Kepler, C. E.: Summary of Recent Hypersonic Inlet Investigations at UAC Research Laboratories. M-1565-2, Res. Labs., United Aircraft Corp., Feb. 1961.
- [REDACTED]

11. McLellan, Charles H., Williams, Thomas W., and Beckwith, Ivan E.: Investigation of the Flow Through a Single-Stage Two-Dimensional Nozzle in the Langley 11-Inch Hypersonic Tunnel. NACA TN 2223, 1950.
12. Bertram, Mitchel H.: Exploratory Investigation of Boundary-Layer Transition on a Hollow Cylinder at a Mach Number of 6.9. NACA Rep. 1313, 1957. (Supersedes NACA TN 3546.)
13. McLellan, Charles H., Williams, Thomas W., and Bertram, Mitchel H.: Investigation of a Two-Step Nozzle in the Langley 11-Inch Hypersonic Tunnel. NACA TN 2171, 1950.
14. Monaghan, R. J.: An Approximate Solution of the Compressible Laminar Boundary Layer on a Flat Plate. R. & M. No. 2760, British A.R.C., 1956.
15. Eckert, E. R. G.: Engineering Relations for Heat Transfer and Friction in High-Velocity Laminar and Turbulent Boundary-Layer Flow Over Surfaces With Constant Pressure and Temperature. Trans. A.S.M.E., vol. 78, no. 6, Aug. 1956, pp. 1273-1283.
16. Persh, Jerome, and Lee, Roland: Tabulation of Compressible Turbulent Boundary Layer Parameters. NAVORD Rep. 4282 (Aeroballistic Res. Rep. 337), U.S. Naval Ord. Lab. (White Oak, Md.), May 1, 1956.

L
1
6
4
3

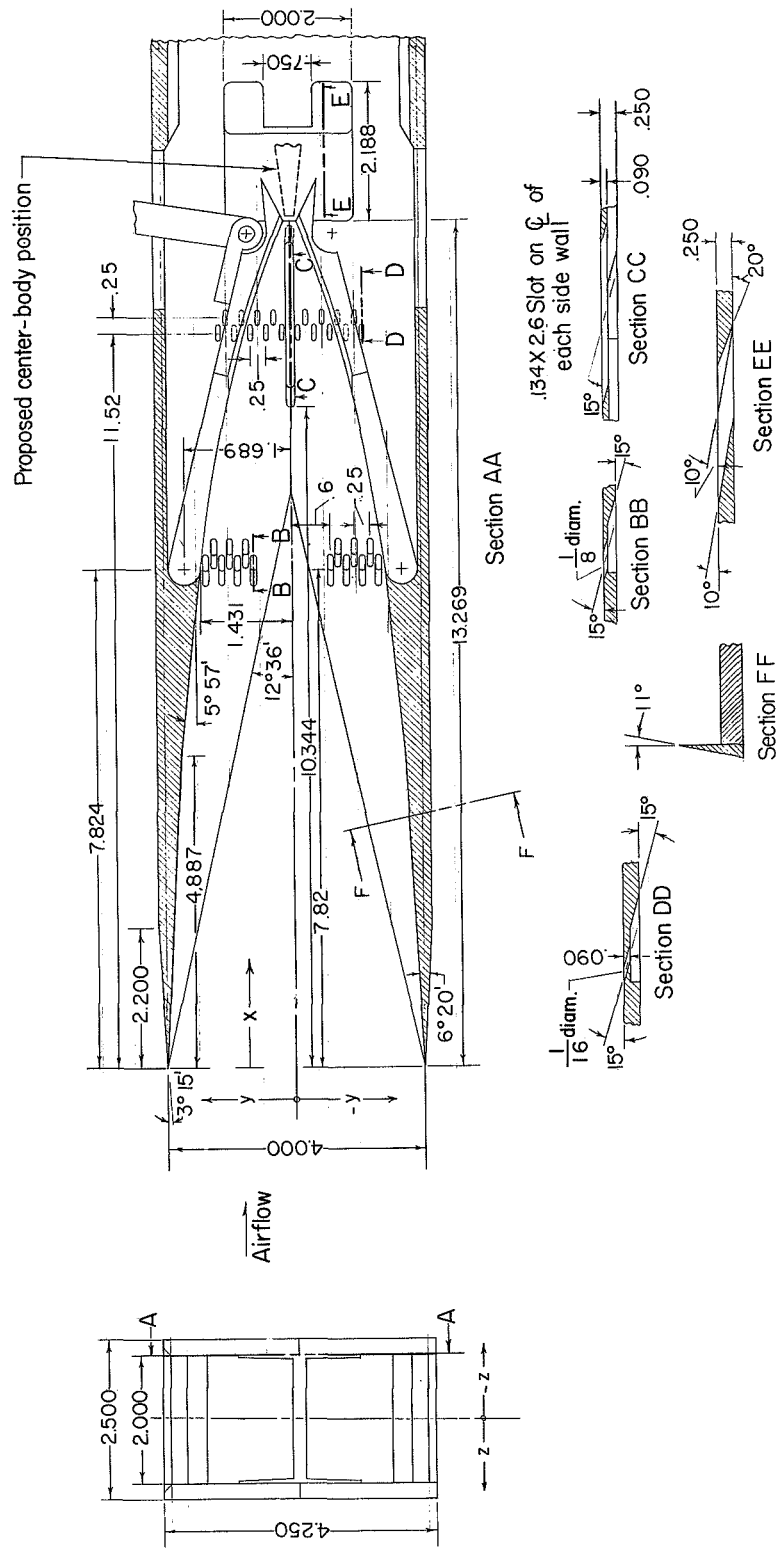
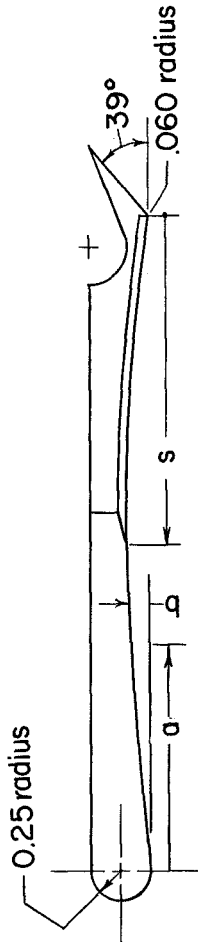


Figure 1.- Inlet model. All dimensions are in inches unless otherwise indicated.

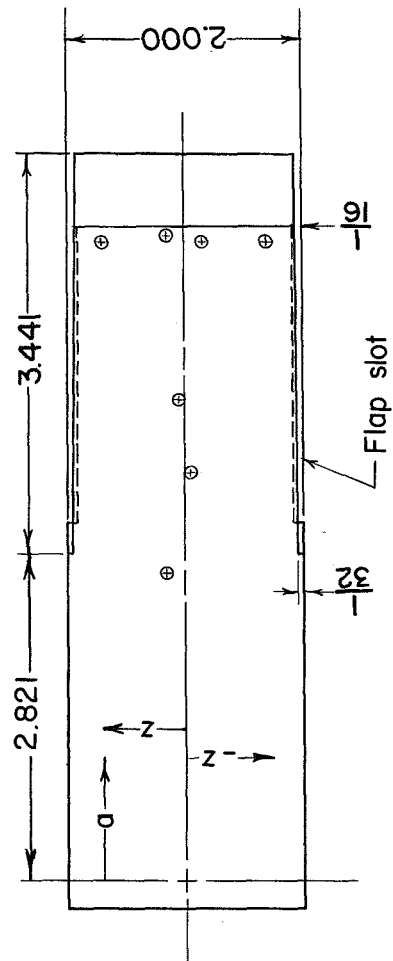
Flap coordinates



Static-pressure-
orifice location

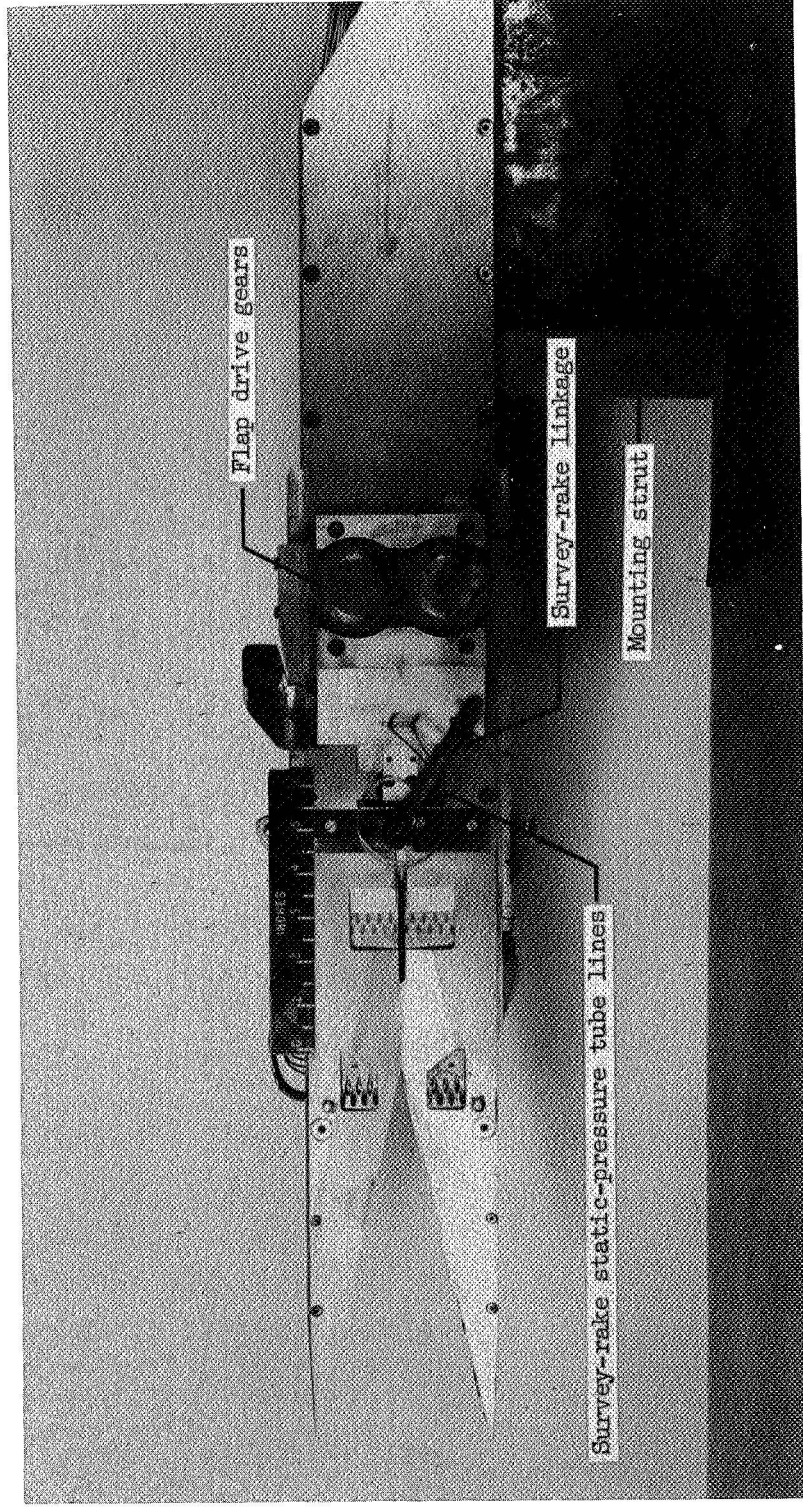
a	z
2.647	.135
3.571	-.045
4.147	.045
5.522	.700
5.522	-.150
5.522	.700
5.584	.150

Note: s = length of flap slot opening



Configuration	s
I, IV	0.000
II, III	2.826 (as shown)
V	1.076

Figure 2.- Flap design. All dimensions are in inches unless otherwise indicated.

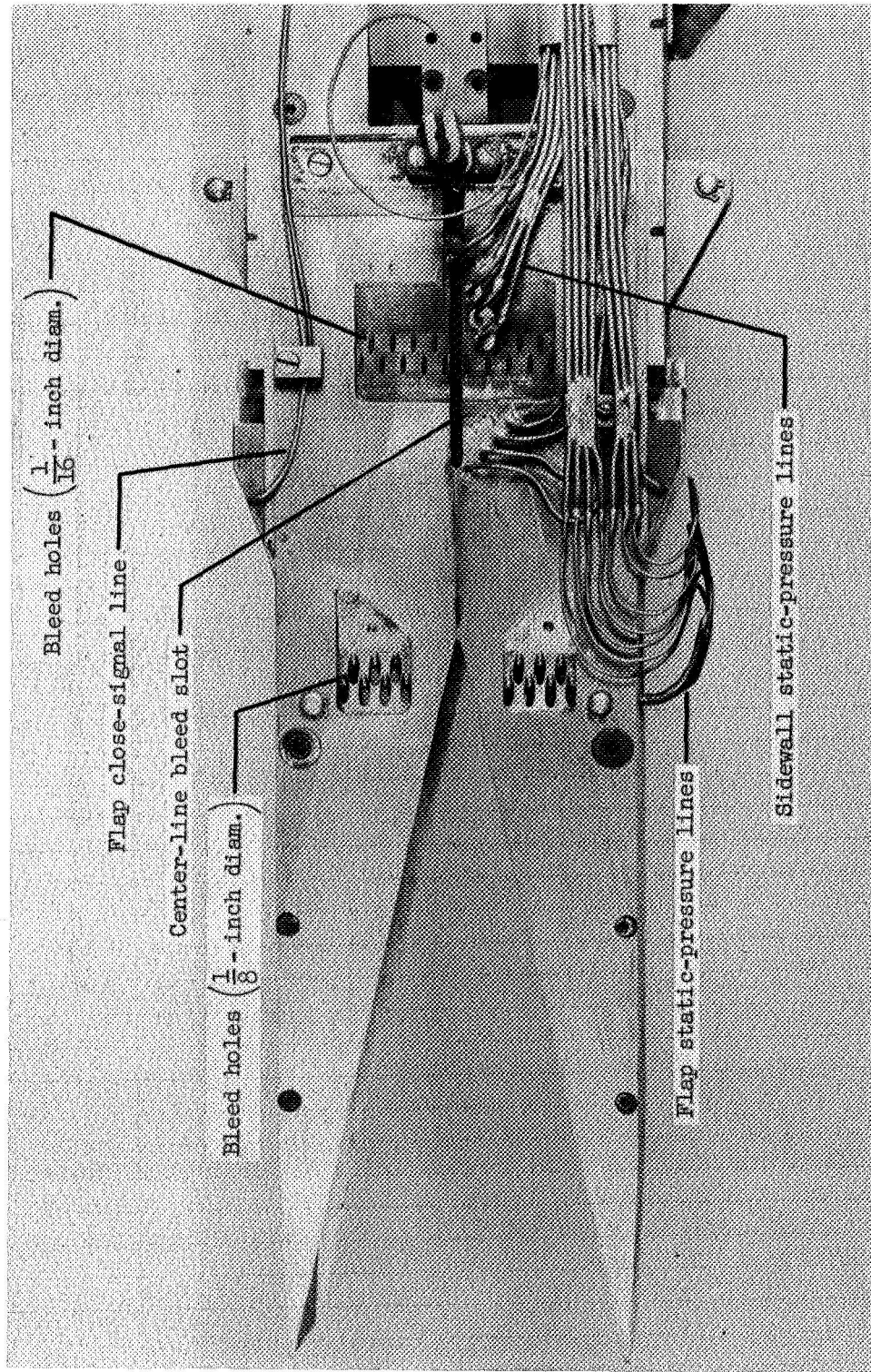


(a) Left side view. L-58-2980.1

Figure 3.- Model used in the investigation.

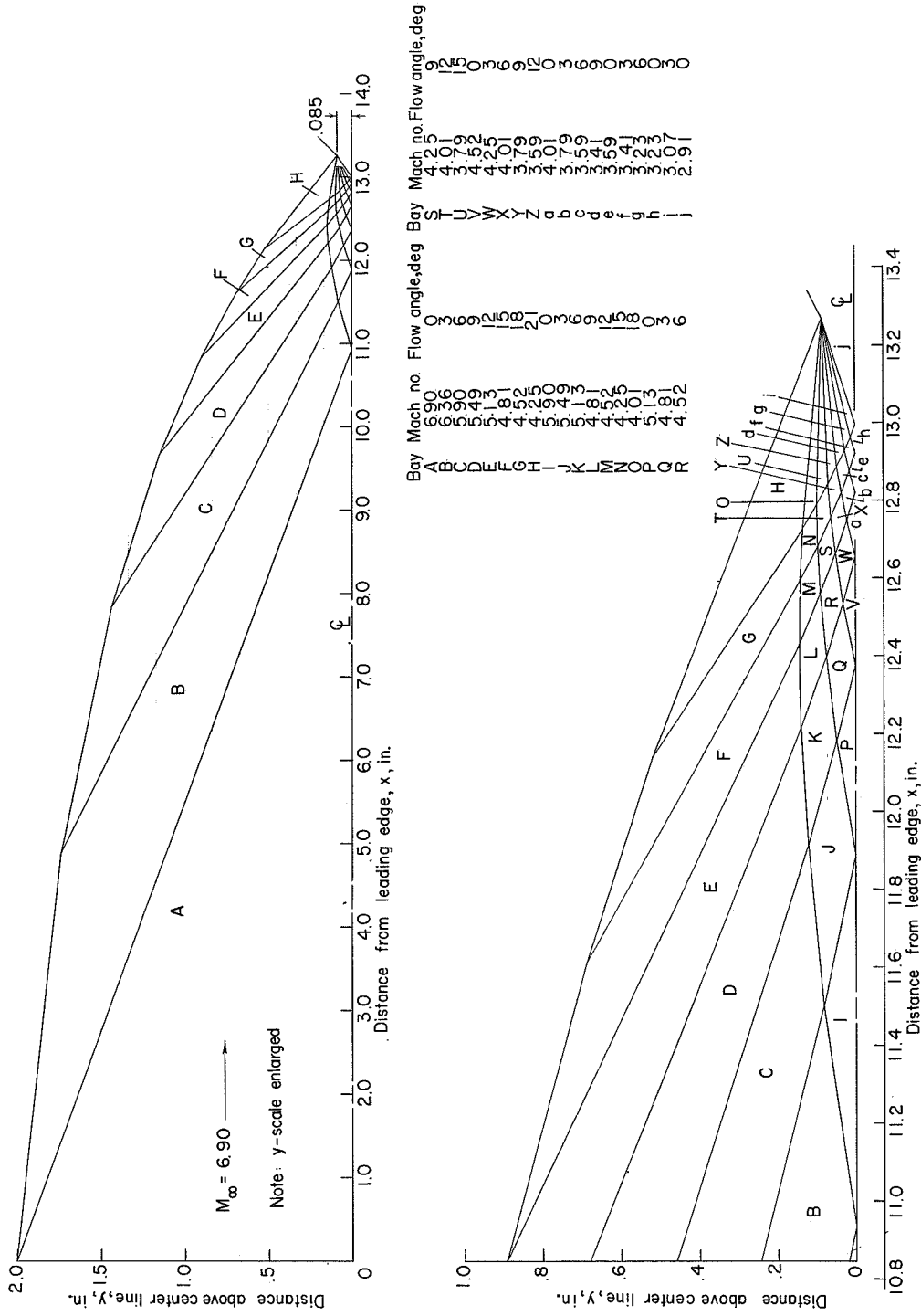
1643

26



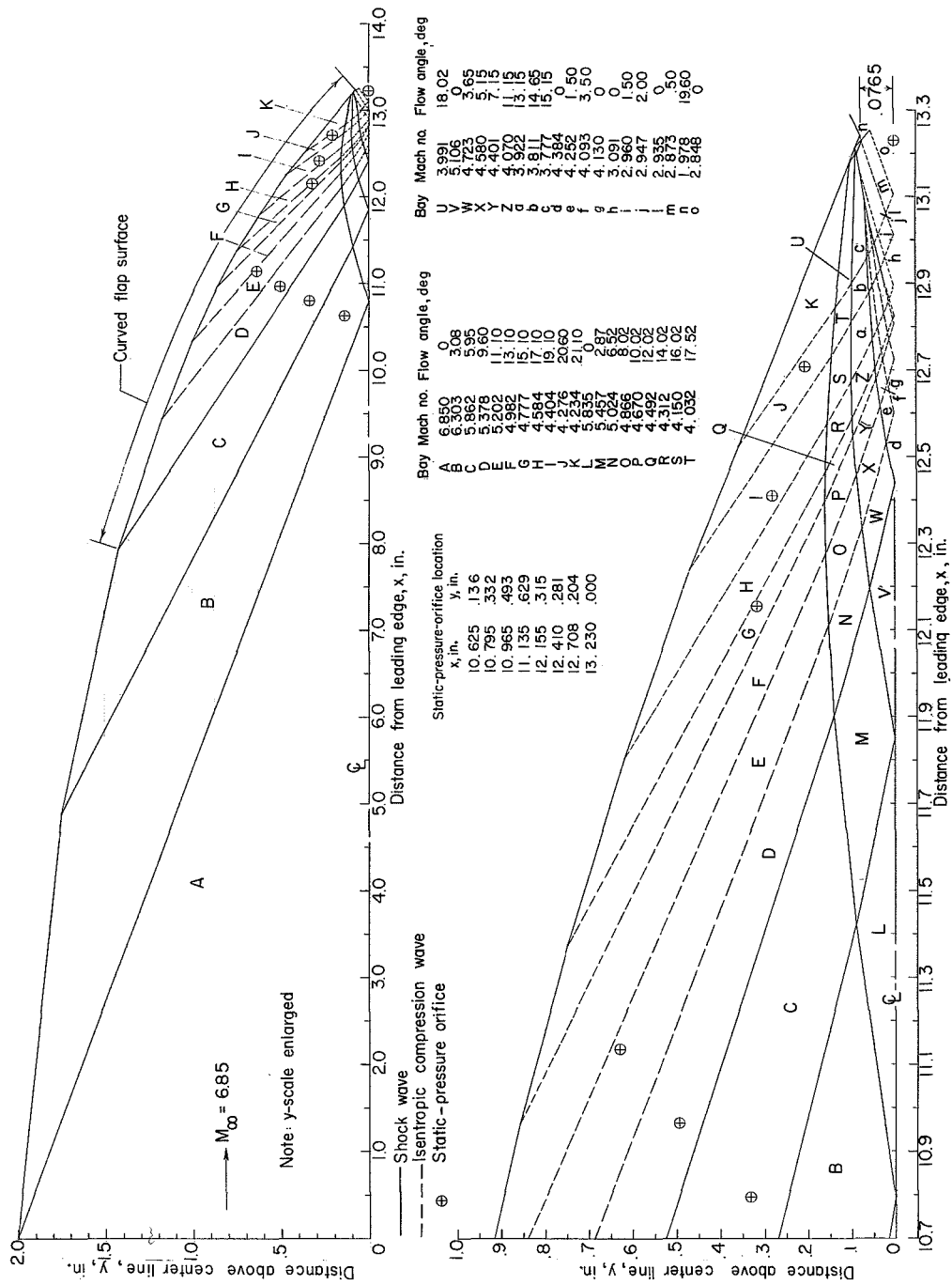
(b) Right side view. L-58-2984.1

Figure 3.- Concluded.



(a) Original design with 14 shocks. $A_\infty/A_T = 23.53$.

Figure 4.- Shock diagrams.



30

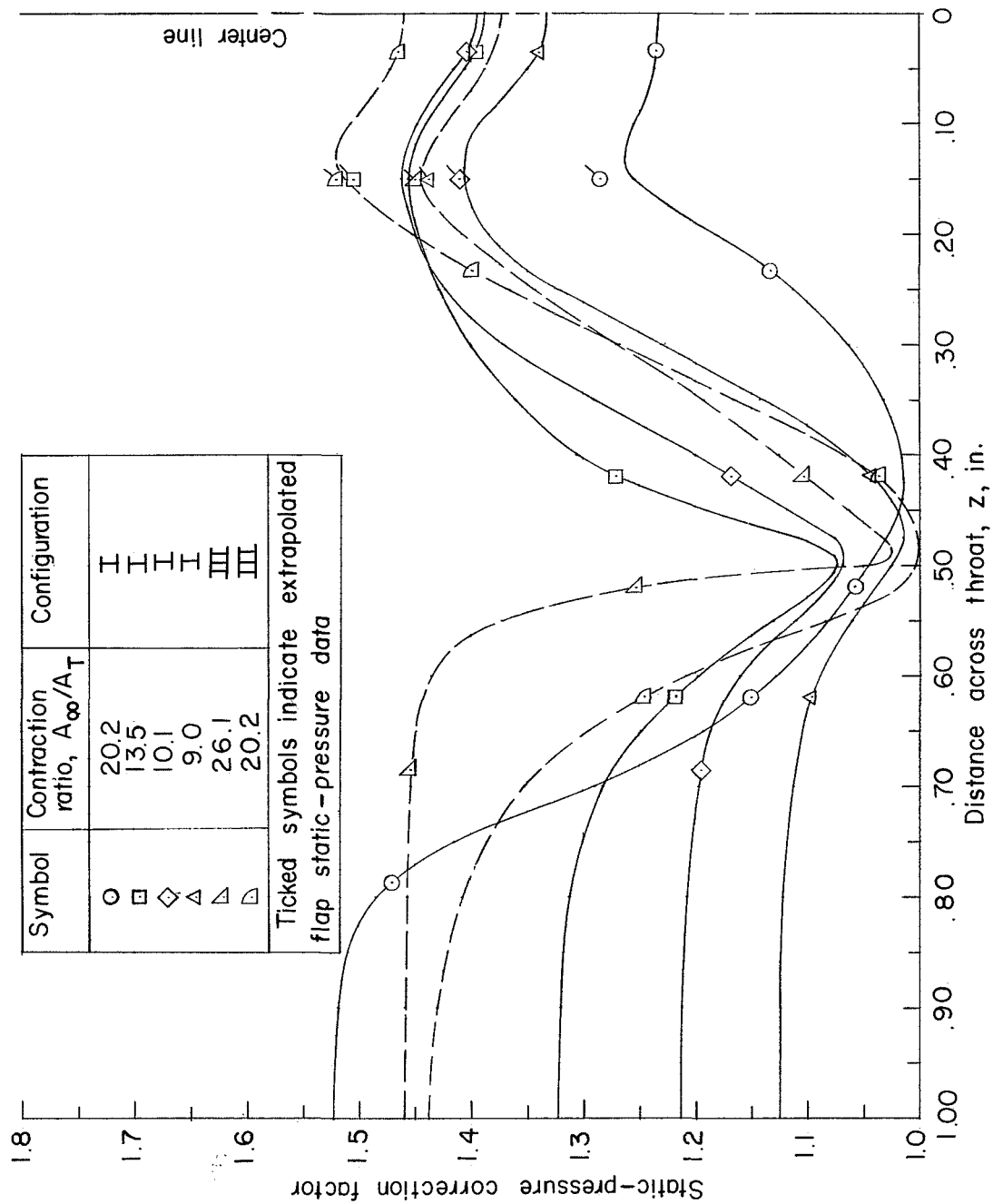


Figure 6.- Static-pressure correction factor.

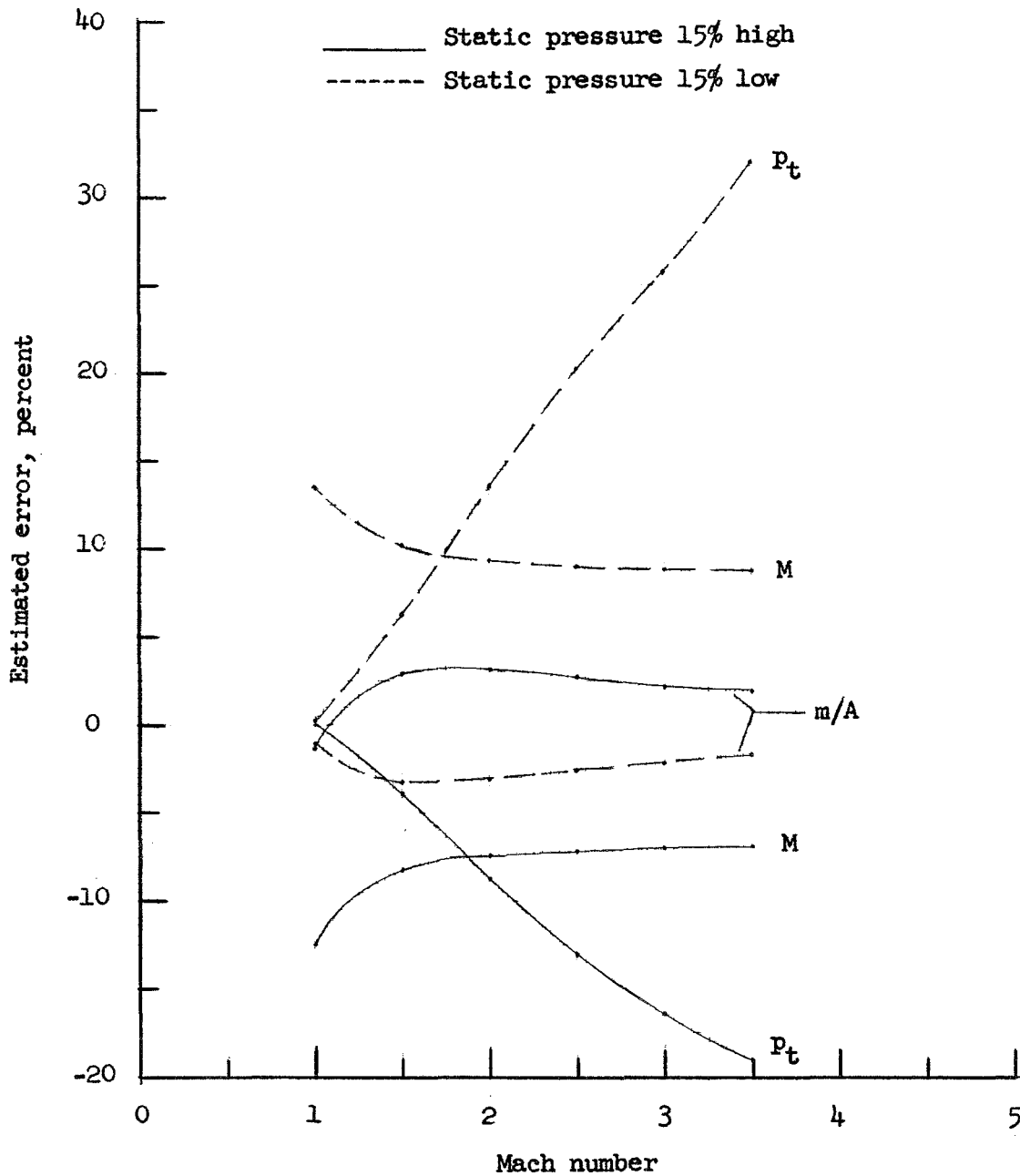
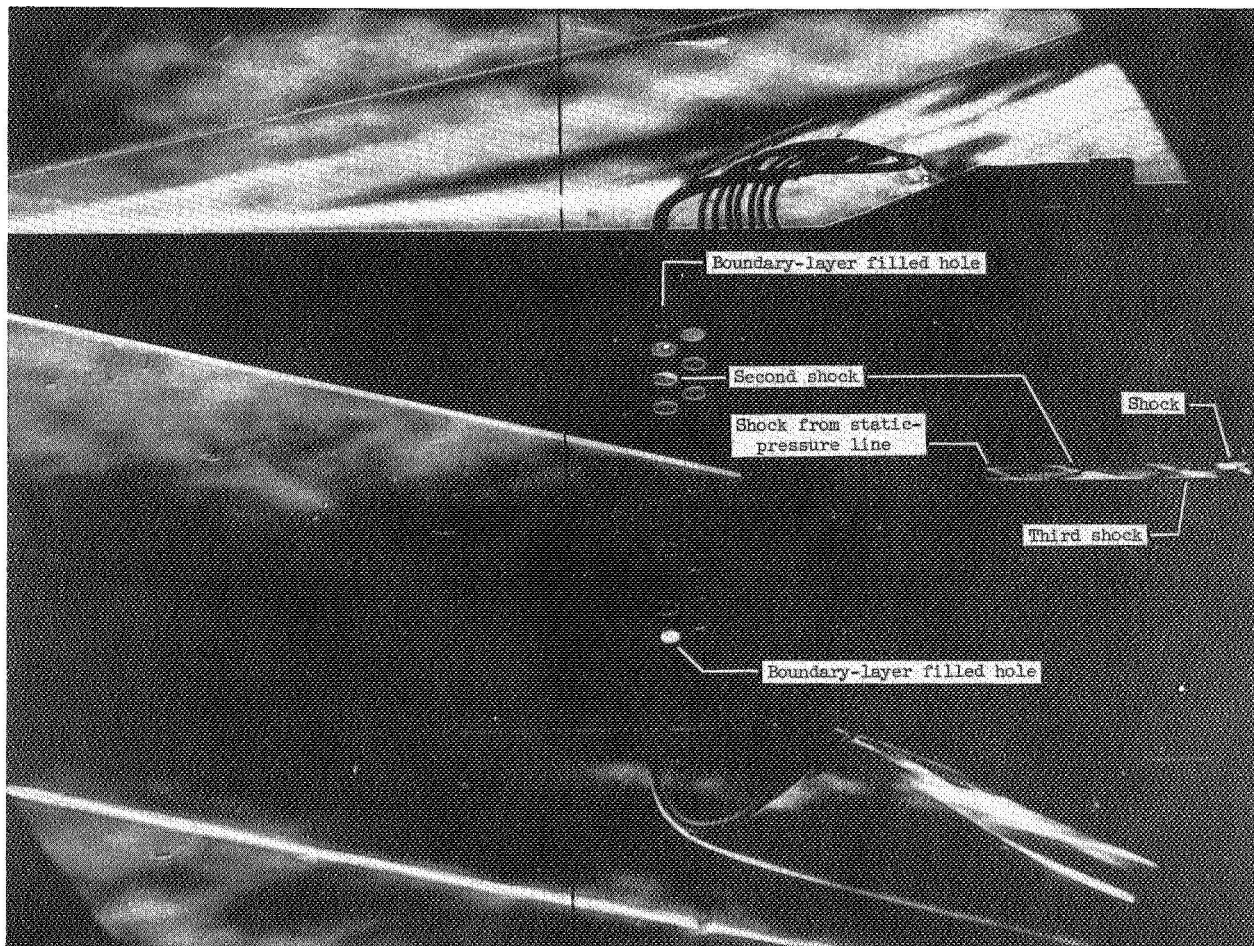


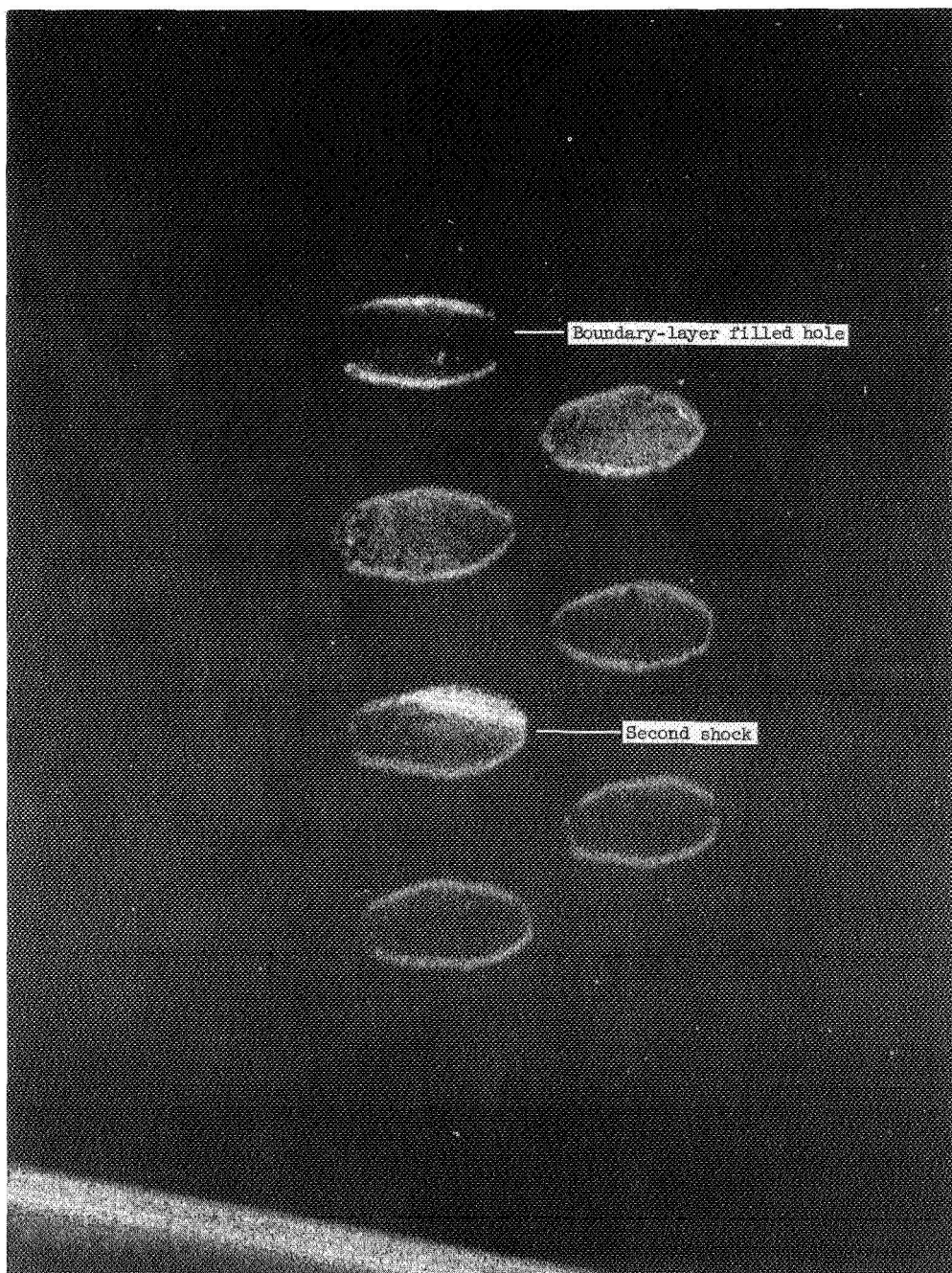
Figure 7.- Estimated maximum errors in point values of parameters due to static-pressure inaccuracies.



(a) Full view.

L-61-5069

Figure 8.- Schlieren observations of shock pattern for configuration I.
 $A_{\infty}/A_T = 20.2$.



(b) Schlieren enlargement of upper group of 1/8-inch-diameter boundary-layer bleed holes.

L-61-5070

Figure 8.- Concluded.

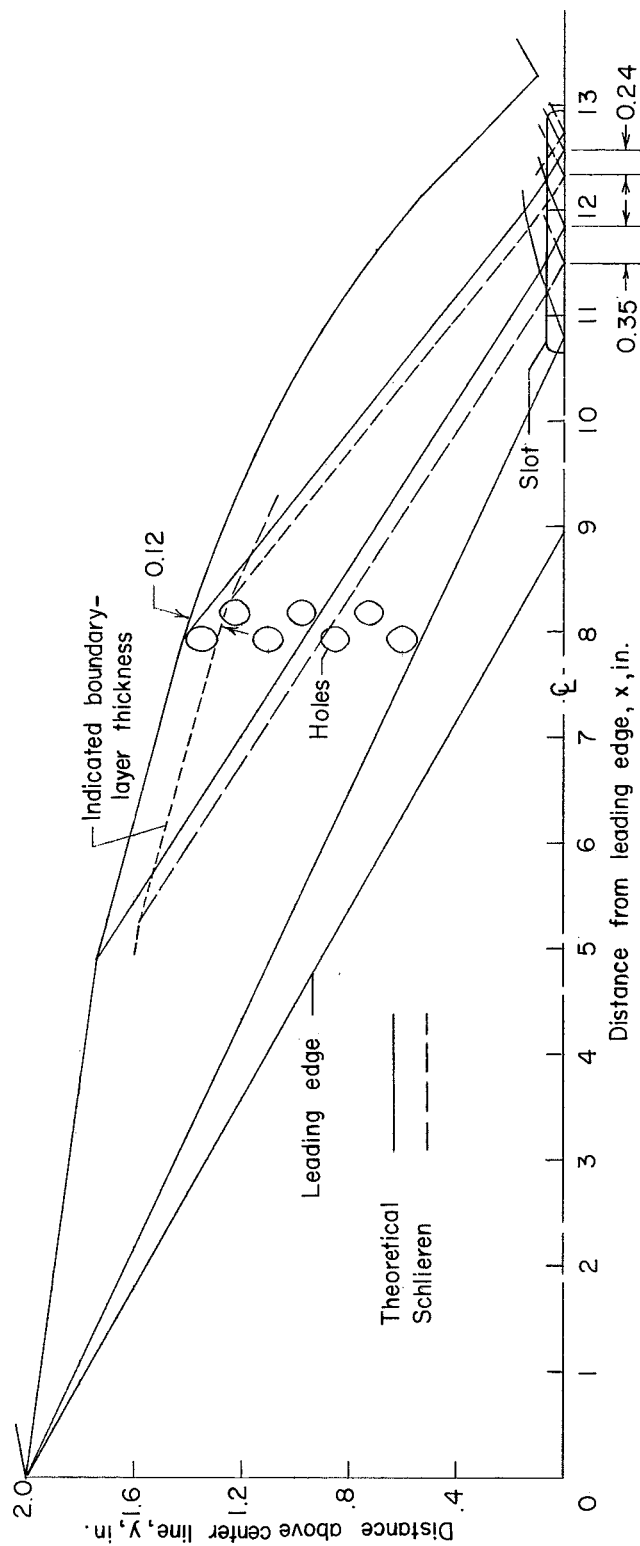
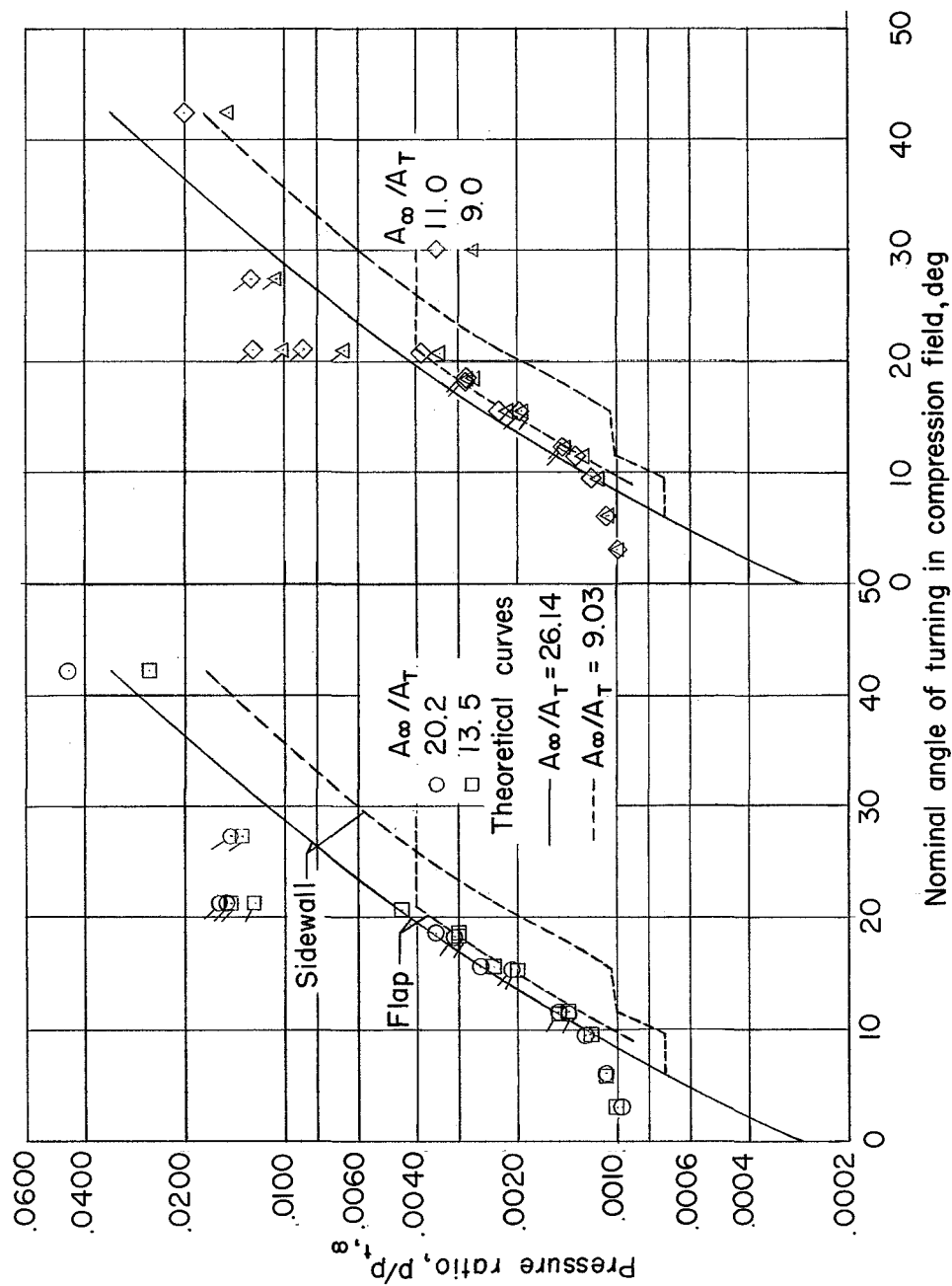
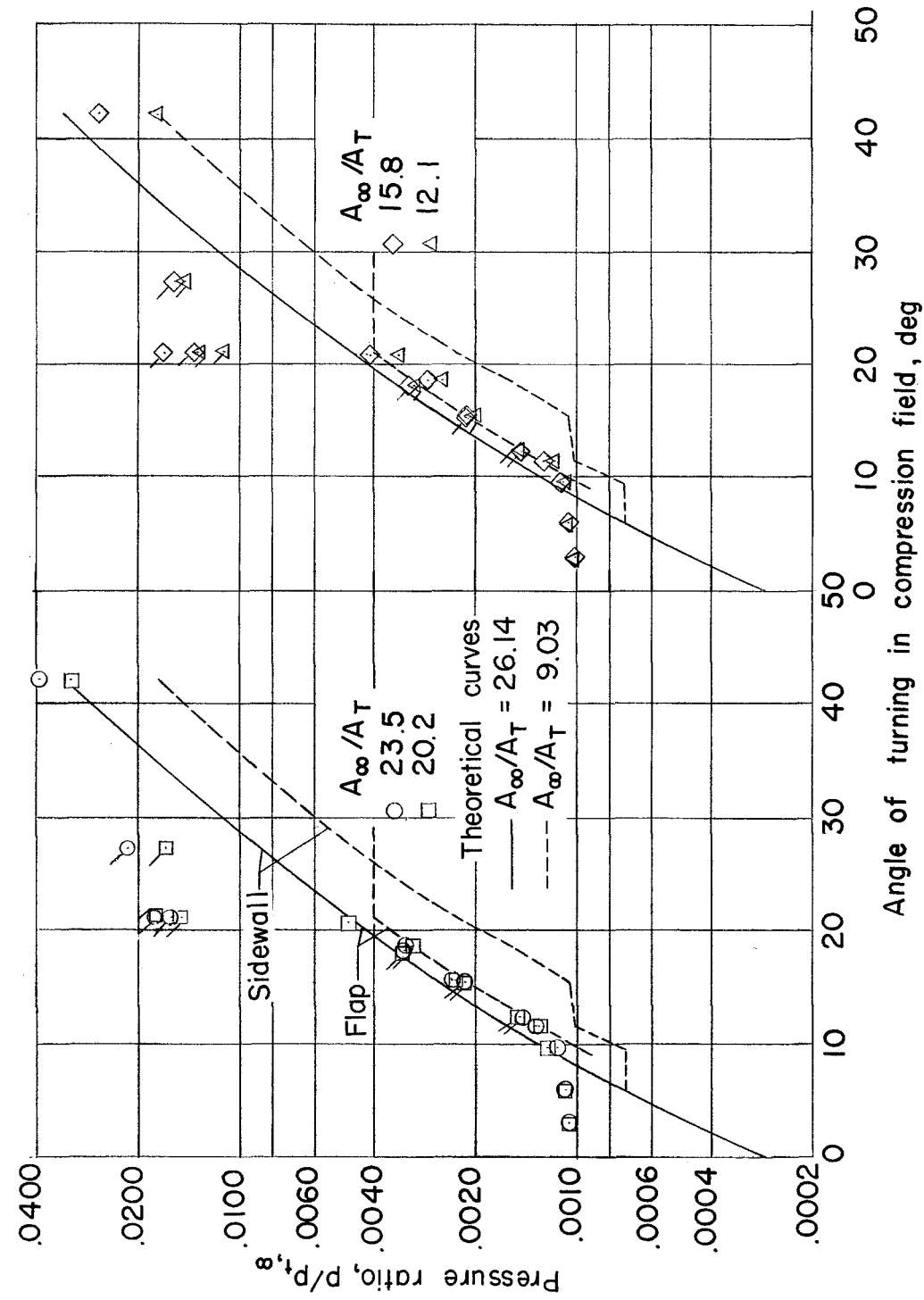


Figure 9.- Comparison of theoretical shock diagram with schlieren observation for configuration I. $A_{\infty}/A_T = 20.2$; y-scale enlarged.



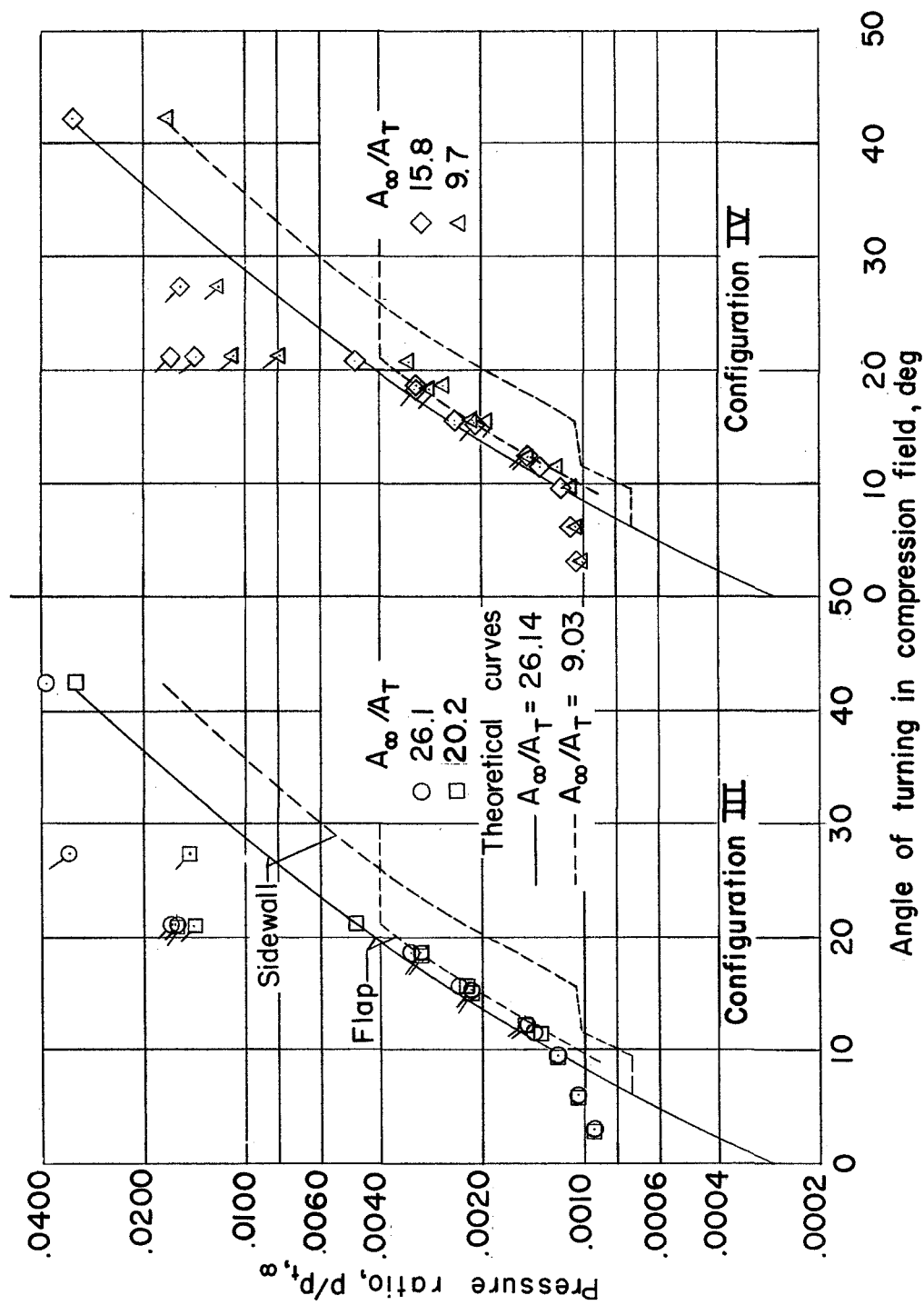
(a) Configuration I.

Figure 10.- Longitudinal wall static-pressure distributions. (Symbols with ticks correspond to flap static pressures.)



(b) Configuration II.

Figure 10.- Continued.



(c) Configurations III and IV.

Figure 10.- Concluded.

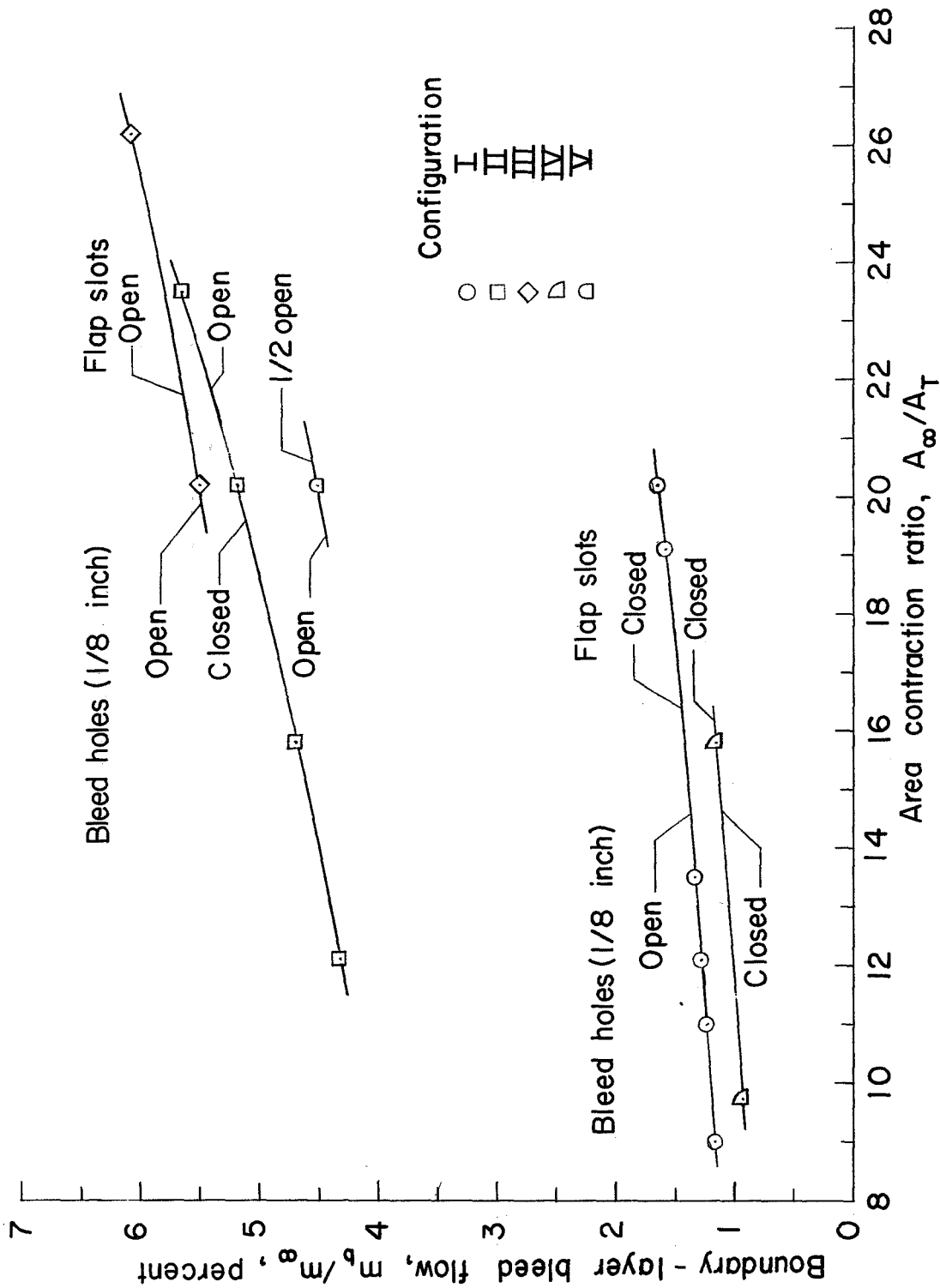
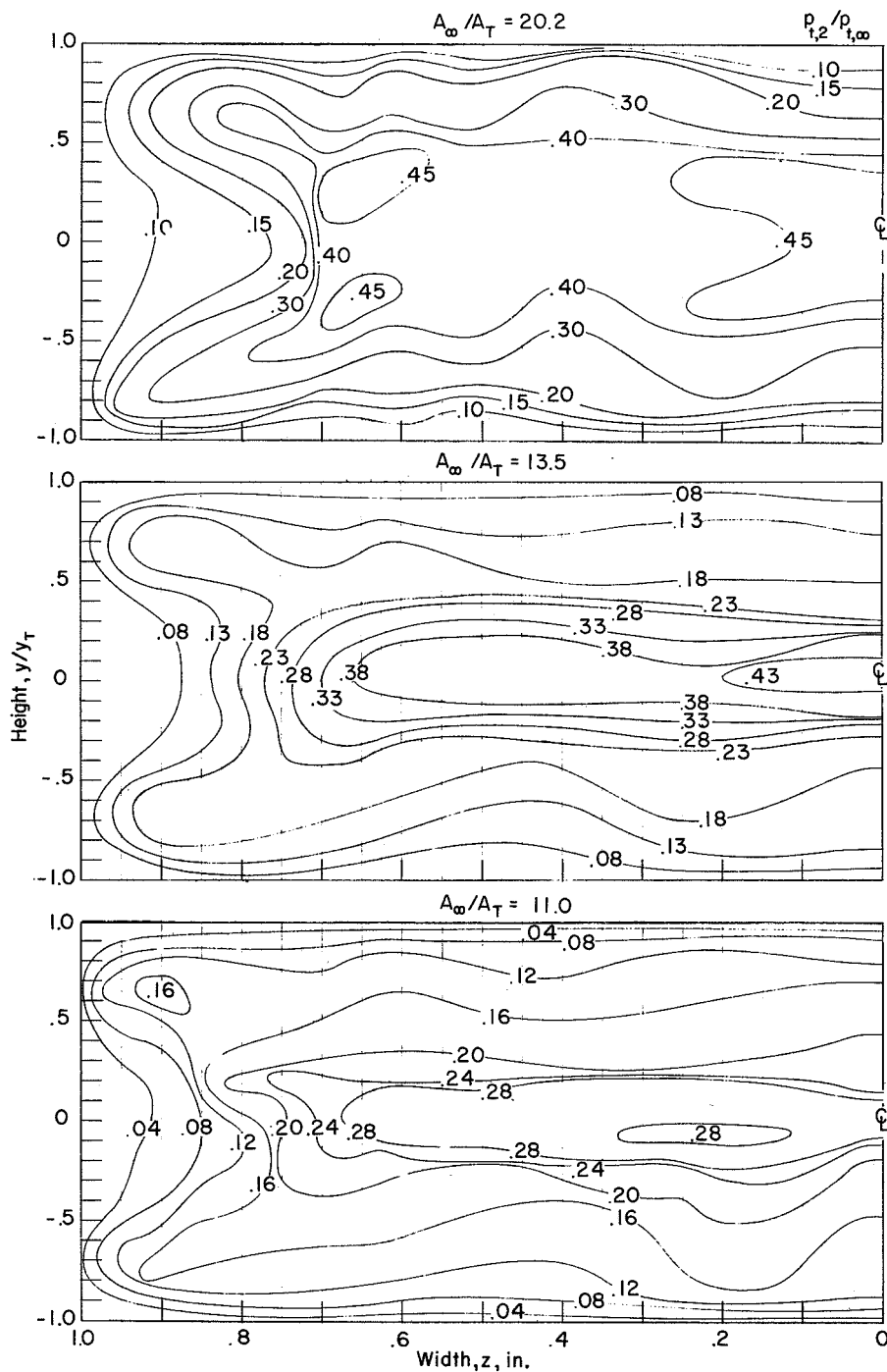


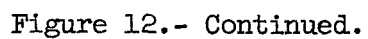
Figure 11.- Computed boundary-layer bleed flows.

I-1645

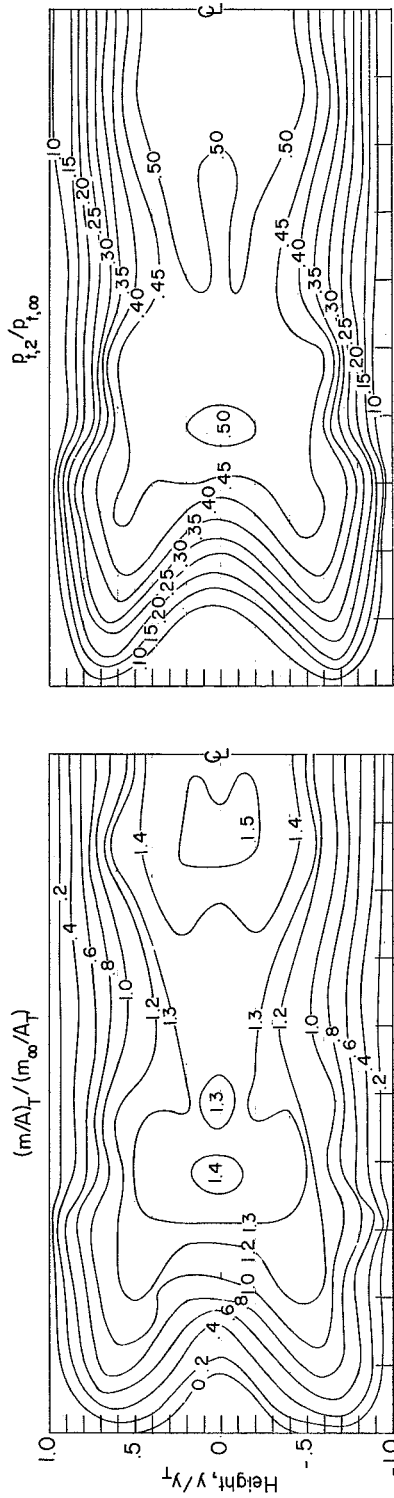


(a) Pitot-stagnation-pressure-recovery contours for configuration I.

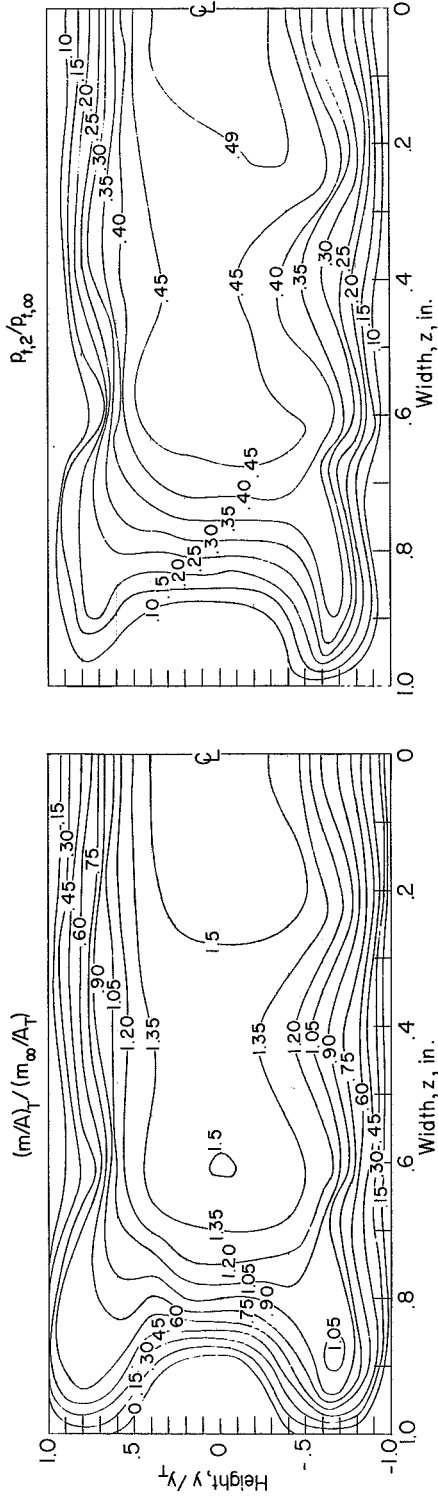
Figure 12.- Contour maps of parameters at throat station.



Configuration III, $A_\infty/A_T = 26.1$



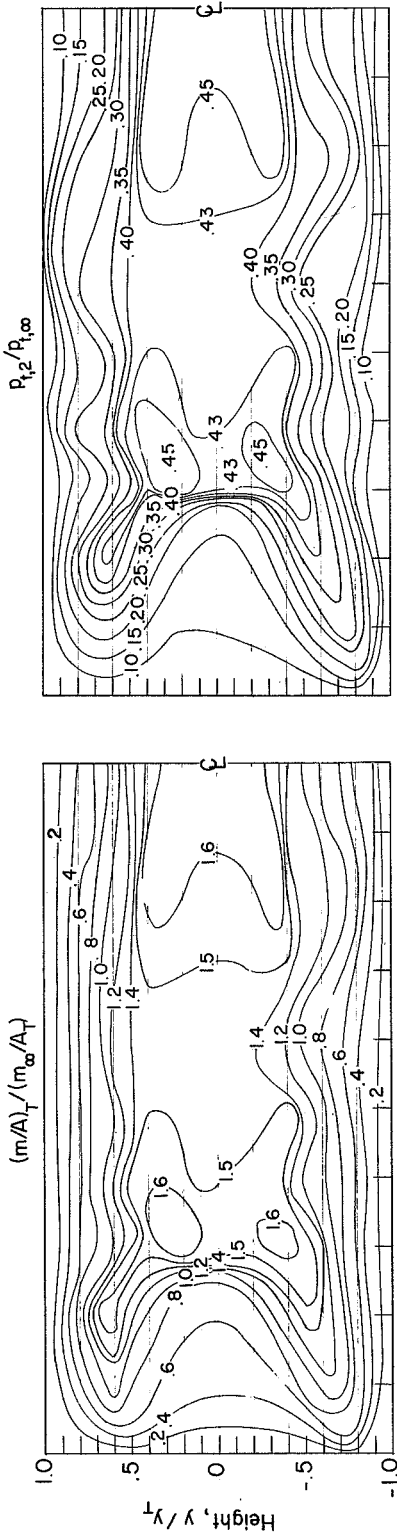
Configuration II, $A_\infty/A_T = 23.5$



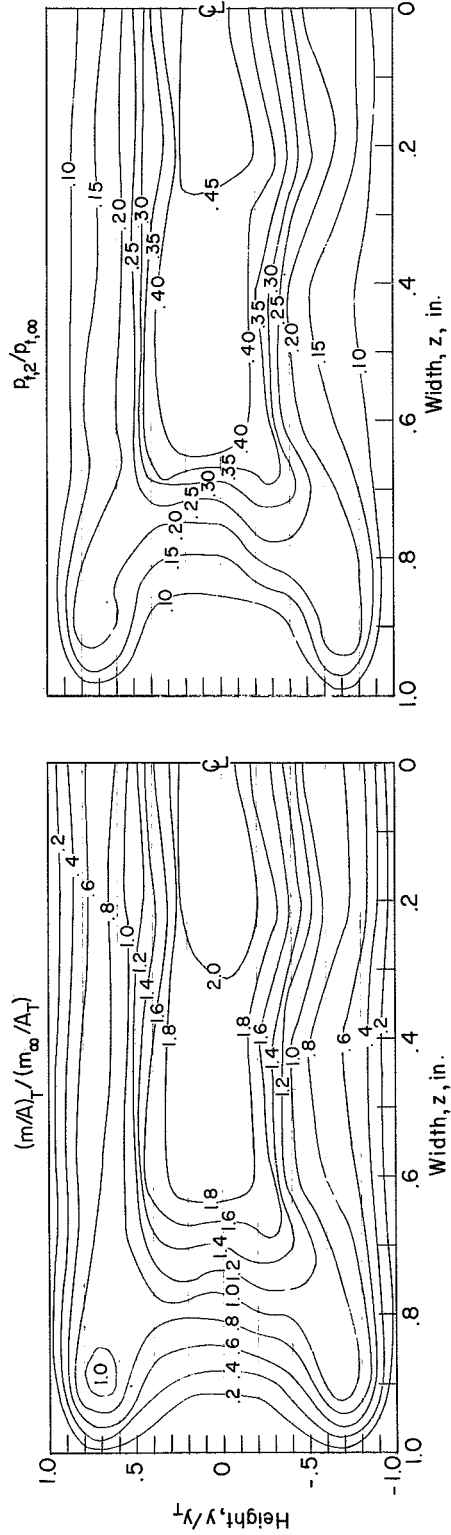
(c) Mass-flow and pitot-stagnation-pressure-recovery contours for highest contraction ratios tested for configurations II and III.

Figure 12.- Continued.

Configuration I, $A_w/A_T = 20.2$



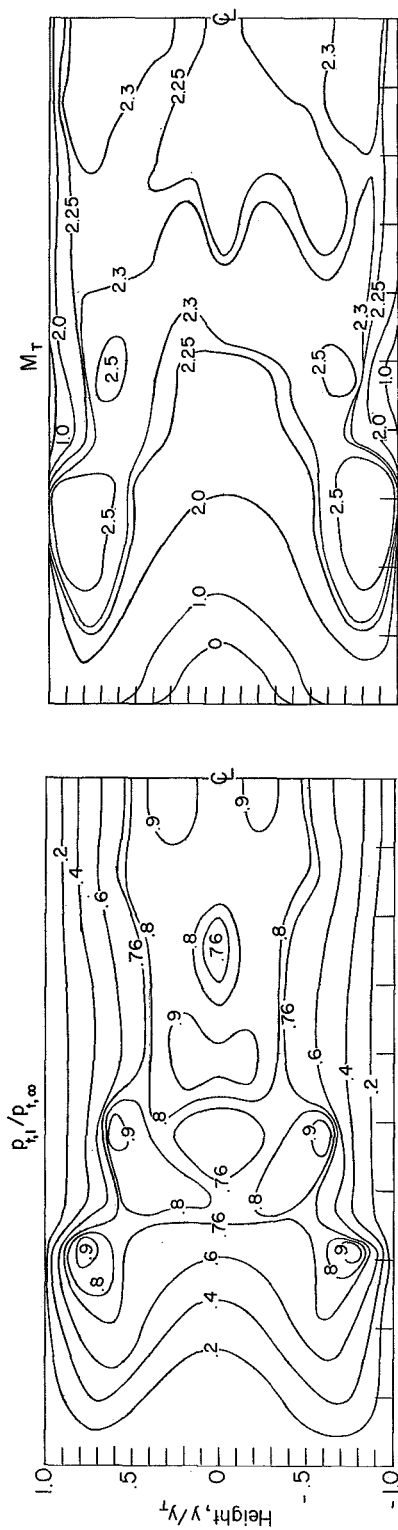
Configuration IV, $A_w/A_T = 15.8$



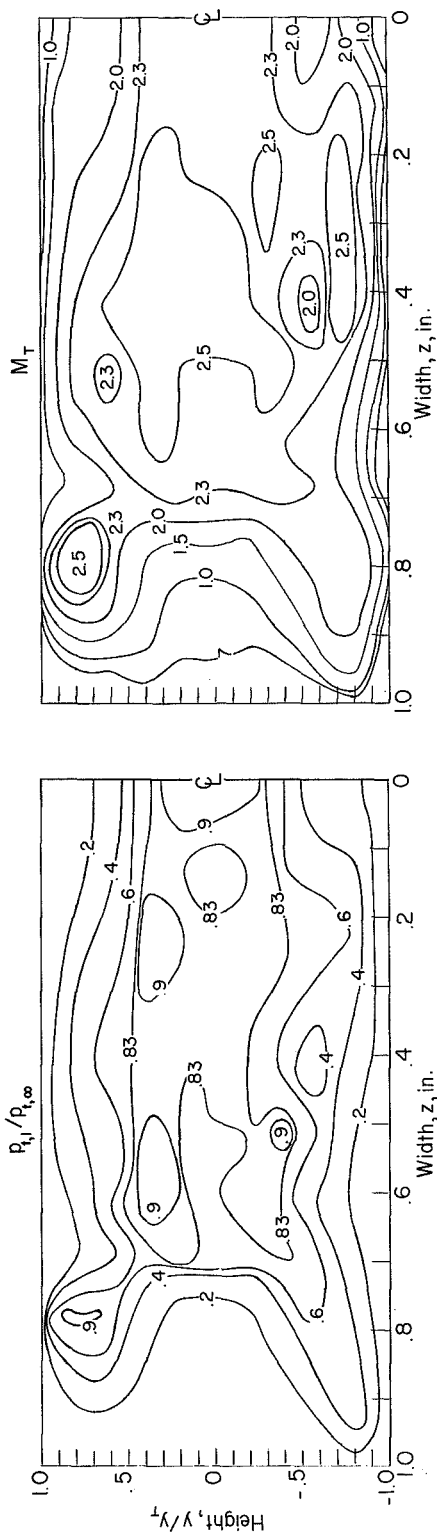
(d) Mass-flow and pitot-stagnation-pressure-recovery contours for highest contraction ratios tested for configurations I and IV.

Figure 12.- Continued.

Configuration III, $A_\infty/A_T = 26.1$



Configuration I, $A_\infty/A_T = 20.2$



(e) Corrected total-pressure recovery and Mach number.

Figure 12.- Concluded.

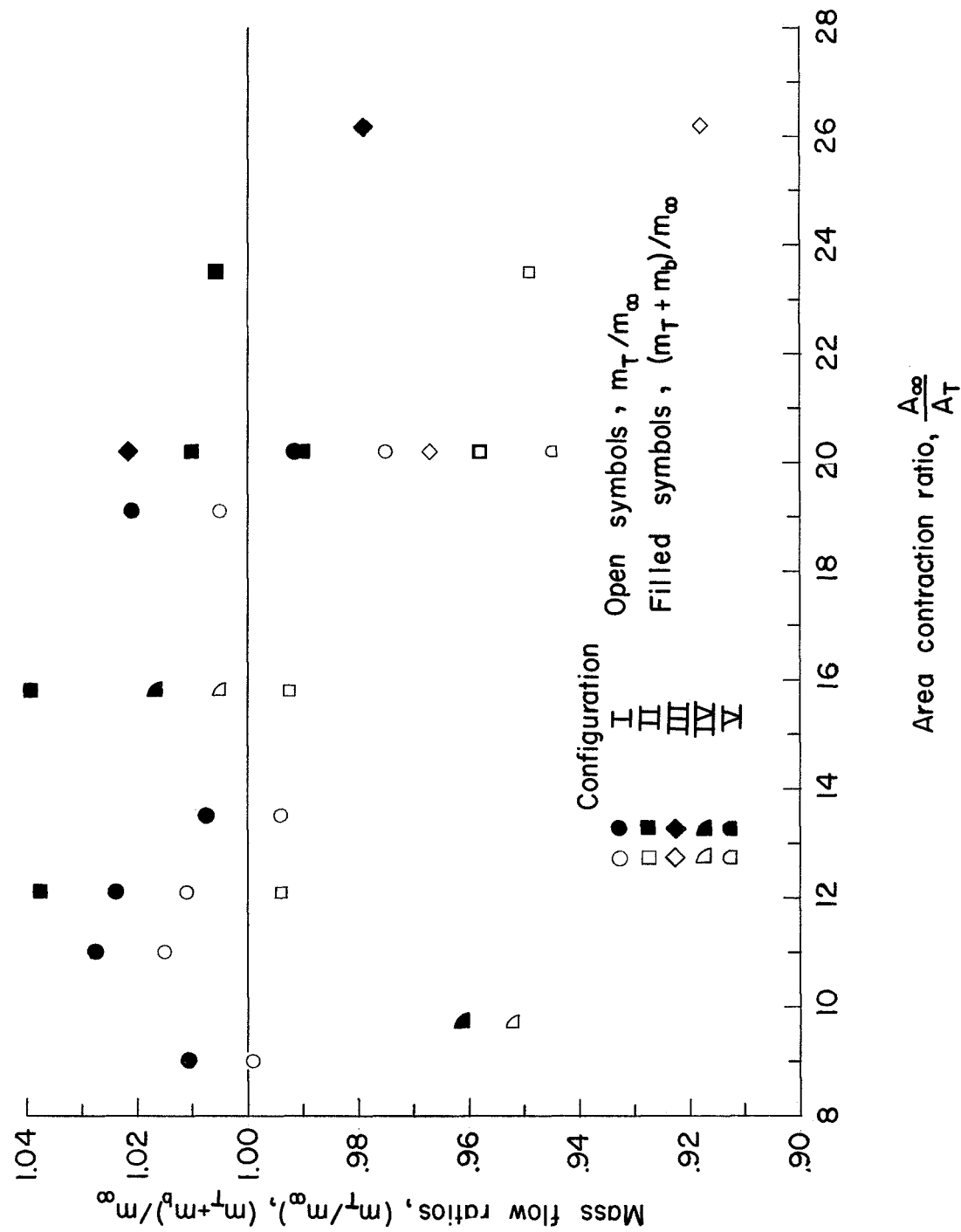


Figure 13.- Throat mass flow ratios determined from integrations of contour maps.

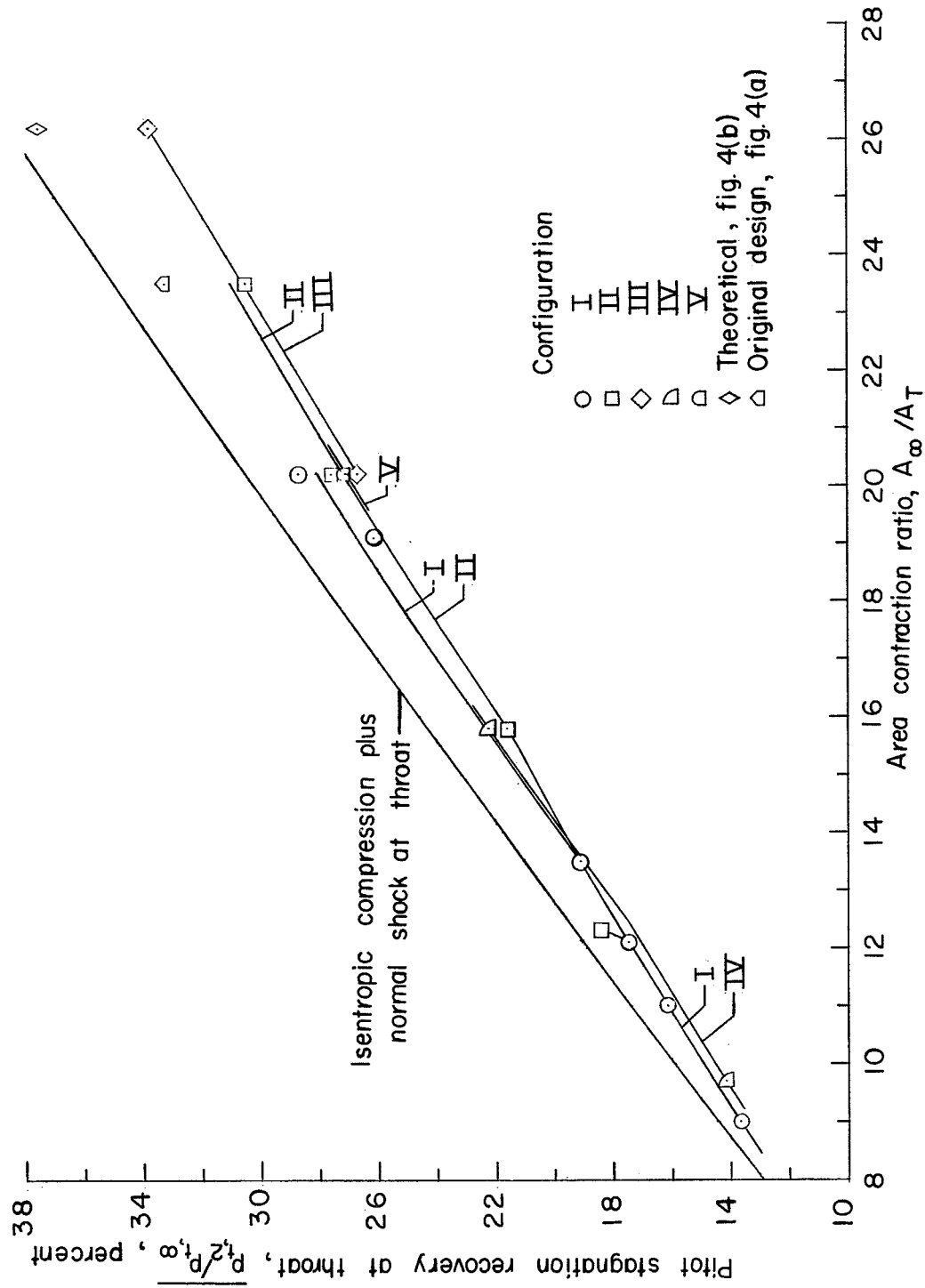


Figure 14.- Average pitot-stagnation-pressure recovery at throat determined from integrations of contour maps.

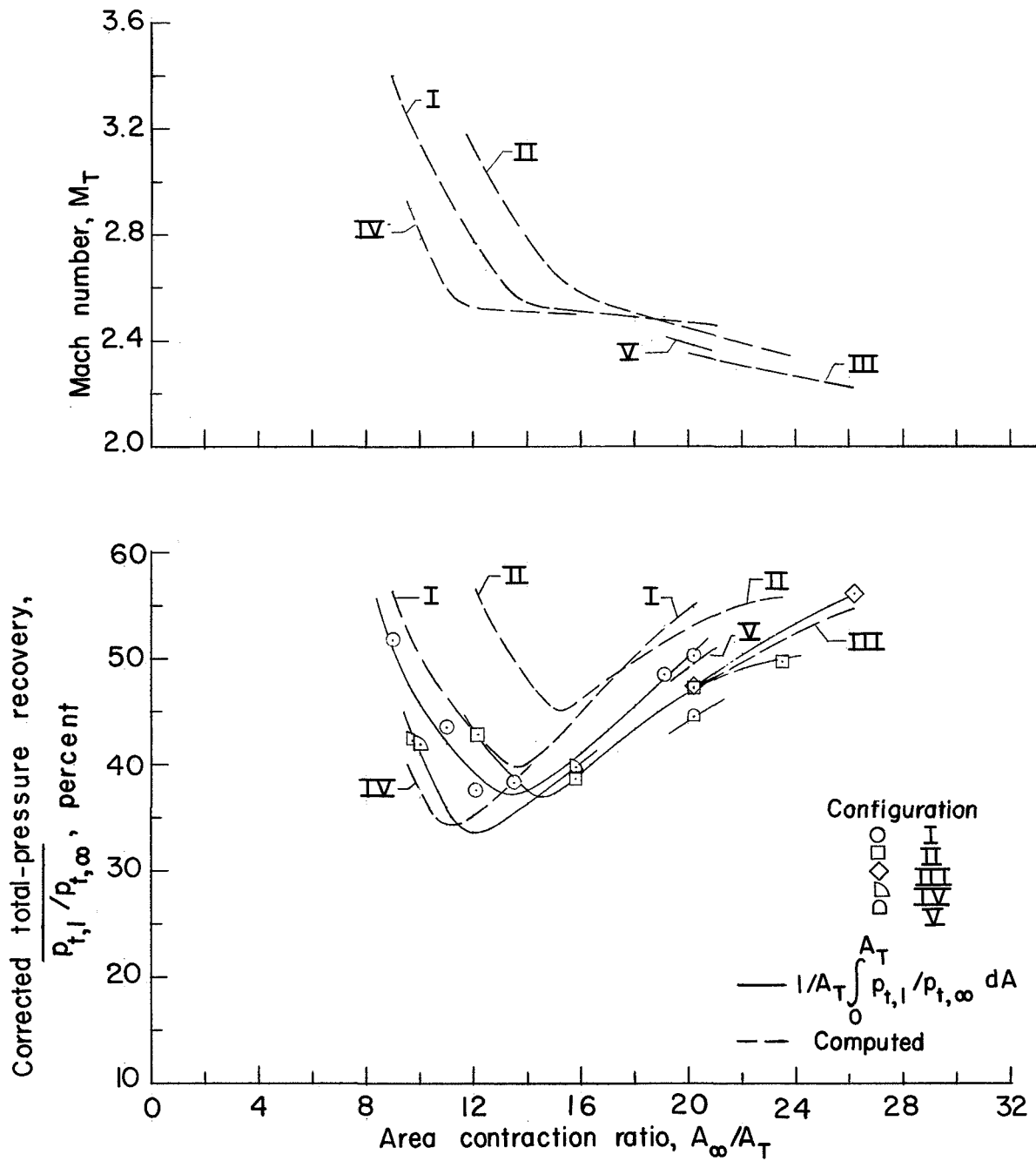


Figure 15.- Corrected total pressure and Mach number at throat.

L-1643

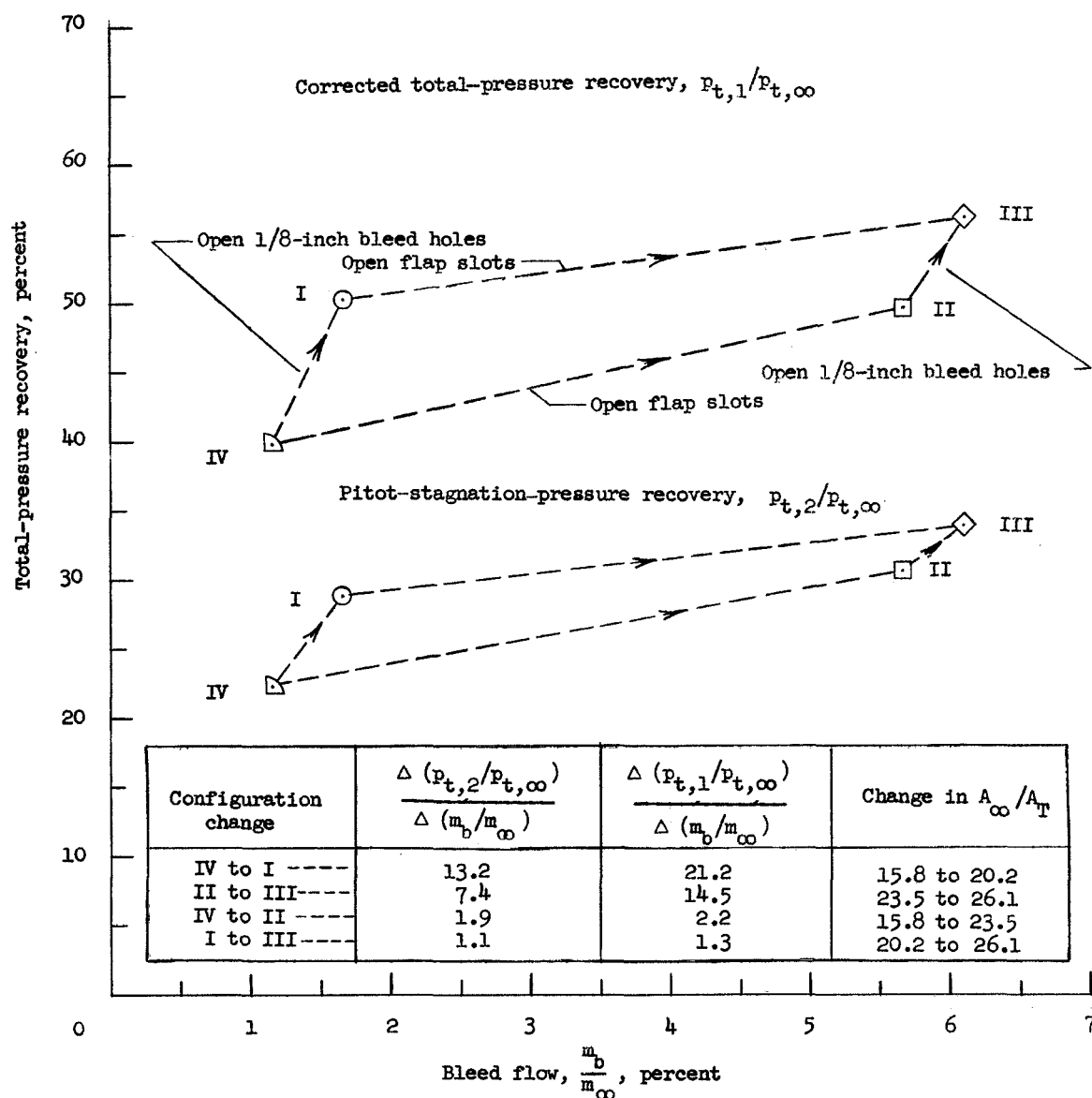


Figure 16.- Effect of boundary-layer bleed on total-pressure recovery for maximum contraction ratios for each configuration.

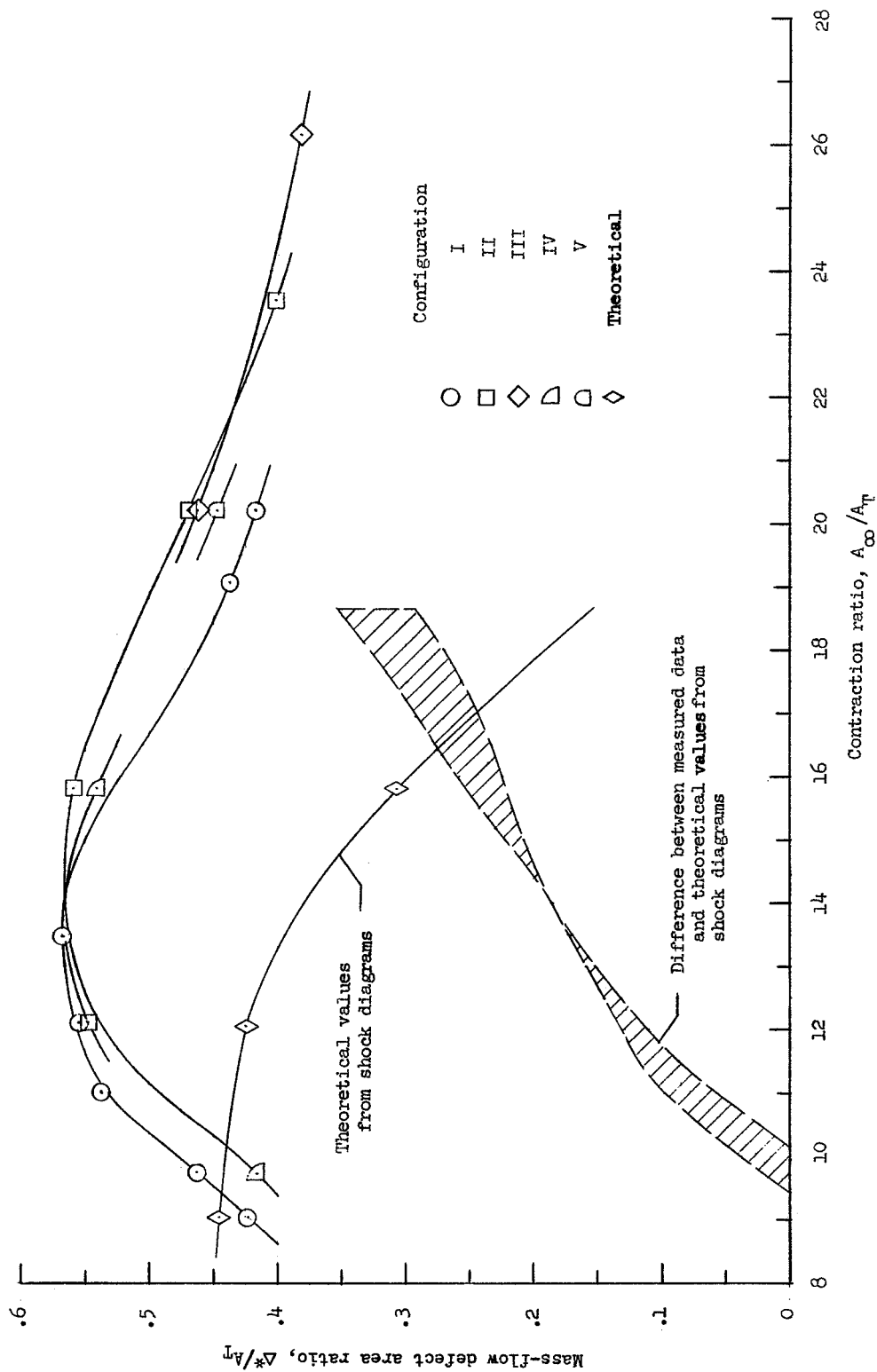


Figure 17.- Mass-flow defect areas at the throat station.

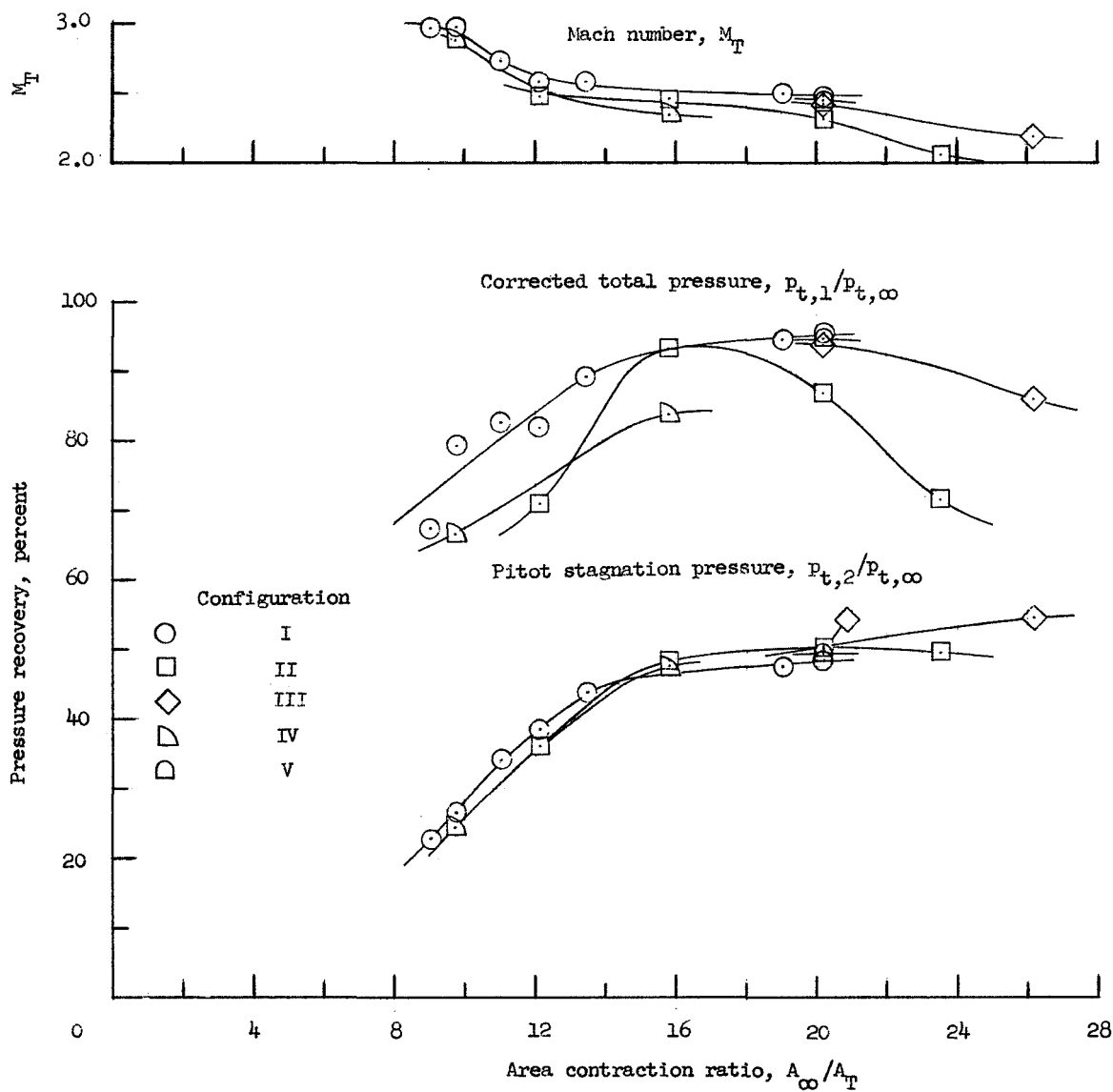


Figure 18.- Conditions at point in throat corresponding to maximum mass flow per unit area.



DECLASSIFIED